

# Measurement of $\mathcal{B}(\Lambda_c^+ \rightarrow pK^-\pi^+)$

CLEO Collaboration  
(November 15, 2018)

## Abstract

The  $\Lambda_c^+ \rightarrow pK^-\pi^+$  yield has been measured in a sample of two-jet continuum events containing both a charm tag (“ $\bar{D}$ ”) as well as an antiproton tag ( $e^+e^- \rightarrow \bar{D}\bar{p}X$ ), with the antiproton in the hemisphere opposite the  $\bar{D}$  (measurement of charge conjugate modes is implicit throughout). Under the hypothesis that such selection criteria tag  $e^+e^- \rightarrow \bar{D}\bar{p}\Lambda_c^+X$  events, the  $\Lambda_c^+ \rightarrow pK^-\pi^+$  branching fraction can be determined by measuring the  $pK^-\pi^+$  yield in the same hemisphere as the antiprotons in our  $\bar{D}\bar{p}X$  sample. Three types of  $\bar{D}$  charm tags are used -  $\pi_{\text{soft}}^-$  (from  $D^{*-} \rightarrow \bar{D}^0\pi_{\text{soft}}^-$ ), electrons (from  $\bar{D} \rightarrow Xe^-\nu$ ), and fully reconstructed  $\bar{D}^0 \rightarrow K^+\pi^-$  or  $D^- \rightarrow K^+\pi^-\pi^-$  or  $D_s^- \rightarrow \phi\pi^-$ . Combining our results obtained from the three independent charm tags, we obtain  $\mathcal{B}(\Lambda_c^+ \rightarrow pK^-\pi^+) = (5.0 \pm 0.5 \pm 1.2)\%$ .

PACS numbers: 13.30.-a, 13.30.Eg, 14.20.Lq

D. E. Jaffe,<sup>1</sup> G. Masek,<sup>1</sup> H. P. Paar,<sup>1</sup> E. M. Potter,<sup>1</sup> S. Prell,<sup>1</sup> V. Sharma,<sup>1</sup> D. M. Asner,<sup>2</sup>  
A. Eppich,<sup>2</sup> J. Gronberg,<sup>2</sup> T. S. Hill,<sup>2</sup> D. J. Lange,<sup>2</sup> R. J. Morrison,<sup>2</sup> R. A. Briere,<sup>3</sup>  
B. H. Behrens,<sup>4</sup> W. T. Ford,<sup>4</sup> A. Gritsan,<sup>4</sup> J. Roy,<sup>4</sup> J. G. Smith,<sup>4</sup> J. P. Alexander,<sup>5</sup>  
R. Baker,<sup>5</sup> C. Bebek,<sup>5</sup> B. E. Berger,<sup>5</sup> K. Berkelman,<sup>5</sup> F. Blanc,<sup>5</sup> V. Boisvert,<sup>5</sup>  
D. G. Cassel,<sup>5</sup> M. Dickson,<sup>5</sup> P. S. Drell,<sup>5</sup> K. M. Ecklund,<sup>5</sup> R. Ehrlich,<sup>5</sup> A. D. Foland,<sup>5</sup>  
P. Gaidarev,<sup>5</sup> L. Gibbons,<sup>5</sup> B. Gittelman,<sup>5</sup> S. W. Gray,<sup>5</sup> D. L. Hartill,<sup>5</sup> B. K. Heltsley,<sup>5</sup>  
P. I. Hopman,<sup>5</sup> C. D. Jones,<sup>5</sup> D. L. Kreinick,<sup>5</sup> M. Lohner,<sup>5</sup> A. Magerkurth,<sup>5</sup> T. O. Meyer,<sup>5</sup>  
N. B. Mistry,<sup>5</sup> C. R. Ng,<sup>5</sup> E. Nordberg,<sup>5</sup> J. R. Patterson,<sup>5</sup> D. Peterson,<sup>5</sup> D. Riley,<sup>5</sup>  
J. G. Thayer,<sup>5</sup> P. G. Thies,<sup>5</sup> B. Valant-Spaight,<sup>5</sup> A. Warburton,<sup>5</sup> P. Avery,<sup>6</sup> C. Prescott,<sup>6</sup>  
A. I. Rubiera,<sup>6</sup> J. Yelton,<sup>6</sup> J. Zheng,<sup>6</sup> G. Brandenburg,<sup>7</sup> A. Ershov,<sup>7</sup> Y. S. Gao,<sup>7</sup>  
D. Y.-J. Kim,<sup>7</sup> R. Wilson,<sup>7</sup> T. E. Browder,<sup>8</sup> Y. Li,<sup>8</sup> J. L. Rodriguez,<sup>8</sup> H. Yamamoto,<sup>8</sup>  
T. Bergfeld,<sup>9</sup> B. I. Eisenstein,<sup>9</sup> J. Ernst,<sup>9</sup> G. E. Gladding,<sup>9</sup> G. D. Gollin,<sup>9</sup> R. M. Hans,<sup>9</sup>  
E. Johnson,<sup>9</sup> I. Karliner,<sup>9</sup> M. A. Marsh,<sup>9</sup> M. Palmer,<sup>9</sup> C. Plager,<sup>9</sup> C. Sedlack,<sup>9</sup> M. Selen,<sup>9</sup>  
J. J. Thaler,<sup>9</sup> J. Williams,<sup>9</sup> K. W. Edwards,<sup>10</sup> R. Janicek,<sup>11</sup> P. M. Patel,<sup>11</sup> A. J. Sadoff,<sup>12</sup>  
R. Ammar,<sup>13</sup> P. Baringer,<sup>13</sup> A. Bean,<sup>13</sup> D. Besson,<sup>13</sup> P. Brabant,<sup>13</sup> M. Cervantes,<sup>13</sup>  
I. Kravchenko,<sup>13</sup> R. P. Stutz,<sup>13</sup> X. Zhao,<sup>13</sup> S. Anderson,<sup>14</sup> V. V. Frolov,<sup>14</sup> Y. Kubota,<sup>14</sup>  
S. J. Lee,<sup>14</sup> R. Mahapatra,<sup>14</sup> J. J. O'Neill,<sup>14</sup> R. Poling,<sup>14</sup> T. Riehle,<sup>14</sup> A. Smith,<sup>14</sup>  
J. Urheim,<sup>14</sup> S. Ahmed,<sup>15</sup> M. S. Alam,<sup>15</sup> S. B. Athar,<sup>15</sup> L. Jian,<sup>15</sup> L. Ling,<sup>15</sup>  
A. H. Mahmood,<sup>15,\*</sup> M. Saleem,<sup>15</sup> S. Timm,<sup>15</sup> F. Wappler,<sup>15</sup> A. Anastassov,<sup>16</sup>  
J. E. Duboscq,<sup>16</sup> K. K. Gan,<sup>16</sup> C. Gwon,<sup>16</sup> T. Hart,<sup>16</sup> K. Honscheid,<sup>16</sup> D. Hufnagel,<sup>16</sup>  
H. Kagan,<sup>16</sup> R. Kass,<sup>16</sup> J. Lorenc,<sup>16</sup> T. K. Pedlar,<sup>16</sup> H. Schwarthoff,<sup>16</sup> E. von Toerne,<sup>16</sup>  
M. M. Zoeller,<sup>16</sup> S. J. Richichi,<sup>17</sup> H. Severini,<sup>17</sup> P. Skubic,<sup>17</sup> A. Undrus,<sup>17</sup> S. Chen,<sup>18</sup>  
J. Fast,<sup>18</sup> J. W. Hinson,<sup>18</sup> J. Lee,<sup>18</sup> N. Menon,<sup>18</sup> D. H. Miller,<sup>18</sup> E. I. Shibata,<sup>18</sup>  
I. P. J. Shipsey,<sup>18</sup> V. Pavlunin,<sup>18</sup> D. Cronin-Hennessy,<sup>19</sup> Y. Kwon,<sup>19,†</sup> A.L. Lyon,<sup>19</sup>  
E. H. Thorndike,<sup>19</sup> C. P. Jessop,<sup>20</sup> H. Marsiske,<sup>20</sup> M. L. Perl,<sup>20</sup> V. Savinov,<sup>20</sup> D. Ugolini,<sup>20</sup>  
X. Zhou,<sup>20</sup> T. E. Coan,<sup>21</sup> V. Fadeyev,<sup>21</sup> I. Korolkov,<sup>21</sup> Y. Maravin,<sup>21</sup> I. Narsky,<sup>21</sup>  
R. Stroynowski,<sup>21</sup> J. Ye,<sup>21</sup> T. Wlodek,<sup>21</sup> M. Artuso,<sup>22</sup> R. Ayad,<sup>22</sup> C. Boulahouache,<sup>22</sup>  
K. Bukin,<sup>22</sup> E. Dambasuren,<sup>22</sup> S. Karamov,<sup>22</sup> S. Kopp,<sup>22</sup> G. Majumder,<sup>22</sup> G. C. Moneti,<sup>22</sup>  
R. Mountain,<sup>22</sup> S. Schuh,<sup>22</sup> T. Skwarnicki,<sup>22</sup> S. Stone,<sup>22</sup> G. Viehhauser,<sup>22</sup> J.C. Wang,<sup>22</sup>  
A. Wolf,<sup>22</sup> J. Wu,<sup>22</sup> S. E. Csorna,<sup>23</sup> I. Danko,<sup>23</sup> K. W. McLean,<sup>23</sup> Sz. Márka,<sup>23</sup> Z. Xu,<sup>23</sup>  
R. Godang,<sup>24</sup> K. Kinoshita,<sup>24,‡</sup> I. C. Lai,<sup>24</sup> S. Schrenk,<sup>24</sup> G. Bonvicini,<sup>25</sup> D. Cinabro,<sup>25</sup>  
L. P. Perera,<sup>25</sup> G. J. Zhou,<sup>25</sup> G. Eigen,<sup>26</sup> E. Lipeles,<sup>26</sup> M. Schmidtler,<sup>26</sup> A. Shapiro,<sup>26</sup>  
W. M. Sun,<sup>26</sup> A. J. Weinstein,<sup>26</sup> F. Würthwein,<sup>26</sup> and

<sup>1</sup>University of California, San Diego, La Jolla, California 92093

<sup>2</sup>University of California, Santa Barbara, California 93106

<sup>3</sup>Carnegie Mellon University, Pittsburgh, Pennsylvania 15213

<sup>4</sup>University of Colorado, Boulder, Colorado 80309-0390

<sup>5</sup>Cornell University, Ithaca, New York 14853

<sup>6</sup>University of Florida, Gainesville, Florida 32611

---

\*Permanent address: University of Texas - Pan American, Edinburg TX 78539.

†Permanent address: Yonsei University, Seoul 120-749, Korea.

‡Permanent address: University of Cincinnati, Cincinnati OH 45221

- <sup>7</sup>Harvard University, Cambridge, Massachusetts 02138
- <sup>8</sup>University of Hawaii at Manoa, Honolulu, Hawaii 96822
- <sup>9</sup>University of Illinois, Urbana-Champaign, Illinois 61801
- <sup>10</sup>Carleton University, Ottawa, Ontario, Canada K1S 5B6  
and the Institute of Particle Physics, Canada
- <sup>11</sup>McGill University, Montréal, Québec, Canada H3A 2T8  
and the Institute of Particle Physics, Canada
- <sup>12</sup>Ithaca College, Ithaca, New York 14850
- <sup>13</sup>University of Kansas, Lawrence, Kansas 66045
- <sup>14</sup>University of Minnesota, Minneapolis, Minnesota 55455
- <sup>15</sup>State University of New York at Albany, Albany, New York 12222
- <sup>16</sup>Ohio State University, Columbus, Ohio 43210
- <sup>17</sup>University of Oklahoma, Norman, Oklahoma 73019
- <sup>18</sup>Purdue University, West Lafayette, Indiana 47907
- <sup>19</sup>University of Rochester, Rochester, New York 14627
- <sup>20</sup>Stanford Linear Accelerator Center, Stanford University, Stanford, California 94309
- <sup>21</sup>Southern Methodist University, Dallas, Texas 75275
- <sup>22</sup>Syracuse University, Syracuse, New York 13244
- <sup>23</sup>Vanderbilt University, Nashville, Tennessee 37235
- <sup>24</sup>Virginia Polytechnic Institute and State University, Blacksburg, Virginia 24061
- <sup>25</sup>Wayne State University, Detroit, Michigan 48202
- <sup>26</sup>California Institute of Technology, Pasadena, California 91125

## I. INTRODUCTION

Of the four fundamental normalization branching fractions of charmed hadrons ( $\mathcal{B}(D^0 \rightarrow K^- \pi^+)$ ,  $\mathcal{B}(D^+ \rightarrow K^- \pi^+ \pi^+)$ ,  $\mathcal{B}(D_s^+ \rightarrow \phi \pi^+)$ , and  $\mathcal{B}(\Lambda_c^+ \rightarrow p K^- \pi^+)$ ),<sup>§</sup> the  $\Lambda_c^+ \rightarrow p K^- \pi^+$  branching fraction is the least well-known, and presently the most controversial. There have been two basic methods used to estimate this branching fraction. The first uses, as input, the ratio of efficiency-corrected yields:  $\frac{\mathcal{B}(\Lambda_c^+ \rightarrow \Lambda X l \nu)}{\mathcal{B}(\Lambda_c^+ \rightarrow p K^- \pi^+)}$  [1,2] and the well-measured  $\Lambda_c^+$  lifetime. One can deduce a total semileptonic branching fraction for  $\Lambda_c^+$  decays

$$\mathcal{B}(\Lambda_c^+ \rightarrow X l \nu) = \frac{\Gamma(\Lambda_c^+ \rightarrow X l \nu)}{\Gamma^{\text{tot}}(\Lambda_c^+)},$$

assuming that the total semileptonic width is the same in  $\Lambda_c^+$  decays as in  $D_s^+ \rightarrow X l \nu$ ,  $D^0 \rightarrow X l \nu$ , and  $D^+ \rightarrow X l \nu$  (the approximate equality of the semileptonic widths for all the charmed mesons lends credence to this assumption, although mass and phase space effects in semileptonic decays may be significant [3]), and assuming  $\frac{\mathcal{B}(\Lambda_c^+ \rightarrow \Lambda X l \nu)}{\mathcal{B}(\Lambda_c^+ \rightarrow X l \nu)} \approx 1.0$  [4–6] (i.e.,  $\frac{\mathcal{B}(\Lambda_c^+ \rightarrow N \bar{K} X l \nu)}{\mathcal{B}(\Lambda_c^+ \rightarrow X l \nu)} \rightarrow 0$ ). Under these assumptions, one can estimate the absolute branching fraction for  $\Lambda_c^+ \rightarrow \Lambda X l \nu$ , and, correspondingly, the absolute branching fraction for  $\Lambda_c^+ \rightarrow p K^- \pi^+$  from the measured  $\frac{\mathcal{B}(\Lambda_c^+ \rightarrow \Lambda X l \nu)}{\mathcal{B}(\Lambda_c^+ \rightarrow p K^- \pi^+)}$  yields. Such a procedure yields values in the range of  $\mathcal{B}(\Lambda_c^+ \rightarrow p K^- \pi^+) \sim 6\text{--}8\%$  [6].

In the second approach, one uses the fact that baryon number must be conserved in  $B$ -decay and that  $\mathcal{B}(b \rightarrow c) \approx 1.0$ . Under the assumption that baryon production in  $B$ -decay occurs through  $\bar{B} \rightarrow \Lambda_c^+ \bar{p} W$ , the observed  $\bar{B} \rightarrow \bar{p} X$  events provide an unbiased sample of  $\bar{B} \rightarrow \Lambda_c^+ X$ . Measurements of the  $\Lambda_c^+ \rightarrow p K^- \pi^+$  yield in such events therefore allow a determination of the absolute  $\Lambda_c^+ \rightarrow p K^- \pi^+$  branching fraction [4,5].\*\* The Particle Data Group uses a combination of this technique and  $D$  and  $\Lambda_c^+$  charm semileptonic measurements to estimate  $\mathcal{B}(\Lambda_c^+ \rightarrow p K^- \pi^+) = (5.0 \pm 1.3)\%$  [7].

In this measurement, we employ a new technique to determine  $\mathcal{B}(\Lambda_c^+ \rightarrow p K^- \pi^+)$  using  $e^+ e^-$  annihilation continuum events. We select a sample of  $e^+ e^- \rightarrow c \bar{c}$  events in which a  $\Lambda_c^+$  is expected to be present by requiring: (i) a charm tag consisting of either a high momentum electron, a  $\pi_{\text{soft}}^-$  (from  $D^{*-} \rightarrow \bar{D}^0 \pi_{\text{soft}}^-$ ), or a fully reconstructed  $\bar{D}$ -meson candidate and (ii) an opposite hemisphere baryon tag consisting of an antiproton. The presence of a  $\Lambda_c^+$  is inferred, to compensate baryon number and charm. According to Monte Carlo simulations, the antiproton in  $\bar{D} \bar{p} \Lambda_c^+$  events is as likely to have its momentum in the same hemisphere as the  $\bar{D}$  as in the hemisphere opposite it. However, estimation of the non- $\Lambda_c^+$  background in our  $\bar{D} \bar{p}(\Lambda_c^+)$  sample is more reliable if we require the antiproton to be in the hemisphere opposite the charm tag. We therefore focus on the sample in which the antiproton is in the hemisphere opposite the charm tag (“ $O(\bar{p}|\bar{D})$ ” events, with parentheses designating opposite hemisphere correlations).<sup>††</sup> Topologically, these events can be schematically depicted as:

---

<sup>§</sup>Charge conjugate modes are implicit.

\*\*Unfortunately, a more recent study of flavor-tagged baryon production in  $B$ -decay indicates that diagrams other than  $\bar{B} \rightarrow \Lambda_c^+ \bar{p} W$  may contribute substantially to  $\Lambda_c^+$ ,  $\bar{\Lambda}_c^-$ , and  $p/\bar{p}$  production in  $B$ -decay [8].

<sup>††</sup>The same-hemisphere  $\bar{p} \bar{D}$  sample, designated with brackets as “ $S[\bar{p} \bar{D}]$ ” is discussed later as a cross-check.

$$\begin{array}{ccc}
 & c \bar{c} & \\
 (\Lambda_c^+) \longleftarrow & & \longrightarrow \bar{D} \\
 \bar{p} \longleftarrow & & 
 \end{array}$$

The yield of  $\Lambda_c^+ \rightarrow pK^-\pi^+$  decays in this  $(\bar{p}|\bar{D})$  sample will allow us, after all the appropriate corrections, to determine the branching fraction:

$$\mathcal{B}(\Lambda_c^+ \rightarrow pK^-\pi^+) = \frac{N(|\bar{p}\Lambda_c^+|\bar{D})}{N(\bar{p}|\bar{D})}.$$

Our analysis comprises two techniques – in one, we construct a three-particle correlation to determine the  $\Lambda_c^+ \rightarrow pK^-\pi^+$  branching fraction, and in the second, a two-particle correlation is sufficient to infer  $\mathcal{B}(\Lambda_c^+ \rightarrow pK^-\pi^+)$ . In the triple correlation analysis, we take the ratio of the number of times that three particles (the  $\Lambda_c^+$ , antiproton, and our charm tag) are found in the same event relative to the number of times that only the antiproton and the charm tag are found. For the second technique, only a double correlation between the reconstructed  $\Lambda_c^+$  and the antiproton tag constitutes the numerator of our ratio; the recoiling charm tag is assumed.

## II. APPARATUS AND EVENT SELECTION

This analysis was performed using the CLEO II detector operating at the Cornell Electron Storage Ring (CESR) at center-of-mass energies  $\sqrt{s} = 10.52\text{--}10.58$  GeV. The CLEO II detector is a general purpose solenoidal magnet spectrometer and calorimeter designed to trigger efficiently on two-photon, tau-pair, and hadronic events [9]. Measurements of charged particle momenta are made with three nested coaxial drift chambers consisting of 6, 10, and 51 layers, respectively. These chambers fill the volume from  $r=3$  cm to  $r=1$  m, with  $r$  being the radial coordinate relative to the beam ( $\hat{z}$ ) axis. This system is very efficient ( $\epsilon \geq 98\%$ ) for detecting tracks that have transverse momenta ( $p_T$ ) relative to the beam axis greater than 200 MeV/ $c$ , and that are contained within the good fiducial volume of the drift chamber ( $|\cos\theta| < 0.94$ , with  $\theta$  defined as the polar angle relative to the beam axis). This system achieves a momentum resolution of  $(\delta p/p)^2 = (0.0015p)^2 + (0.005)^2$  ( $p$  is the momentum, measured in GeV/ $c$ ). Pulse height measurements in the main drift chamber provide specific ionization resolution of 5.5% for Bhabha events, giving good  $K/\pi$  separation for tracks with momenta up to 700 MeV/ $c$  and separation of order  $2\sigma$  in the relativistic rise region above 2 GeV/ $c$ . Outside the central tracking chambers are plastic scintillation counters, which are used as a fast element in the trigger system and also provide particle identification information from time-of-flight measurements.

Beyond the time-of-flight system is the electromagnetic calorimeter, consisting of 7800 thallium-doped CsI crystals. The central “barrel” region of the calorimeter covers about 75% of the solid angle and has an energy resolution which is empirically found to follow

$$\frac{\sigma_E}{E}(\%) = \frac{0.35}{E^{0.75}} + 1.9 - 0.1E; \tag{1}$$

$E$  is the shower energy in GeV. This parameterization includes effects such as noise, and translates to an energy resolution of about 4% at 100 MeV and 1.2% at 5 GeV. Two end-cap regions of the crystal calorimeter extend solid angle coverage to about 95% of  $4\pi$ , although energy resolution is not as good as that of the barrel region. The tracking system, time-of-flight counters, and calorimeter

are all contained within a superconducting coil operated at 1.5 Tesla. Flux return and tracking chambers used for muon detection are located immediately outside the coil and in the two end-cap regions.

The event sample used for this measurement is comprised of  $3.1 \text{ fb}^{-1}$  of data collected at the  $\Upsilon(4S)$  resonance and  $1.6 \text{ fb}^{-1}$  of data collected about 60 MeV below the  $\Upsilon(4S)$  resonance. Approximately  $5 \times 10^6$  continuum  $c\bar{c}$  events are included in this sample.

### A. Event Selection Criteria

In order to suppress background and enrich the hadronic fraction of our event sample, we impose several event requirements. Candidate events must have: (1) at least four detected, good quality, charged tracks; (2) an event vertex consistent with the known  $e^+e^-$  interaction point; (3) a total measured visible event energy, defined as the sum of the measured energy carried by charged tracks plus the measured energy carried by neutral particles ( $E_{\text{vis}} = E_{\text{chrg}} + E_{\text{neutral}}$ ) greater than 110% of the single beam energy,  $E_{\text{vis}} > 1.1 \cdot E_{\text{beam}}$ . In addition, when using an electron to tag a  $c\bar{c}$  event we require that either the beam energy  $E_{\text{beam}}$  be less than 5.275 GeV (below the  $\Upsilon(4S) \rightarrow B\bar{B}$  threshold) or that the event be well collimated. Specifically, the ratio of Fox-Wolfram event shape parameters  $H2/H0$  can be used to quantify the “jettiness” of an event [10] – for a perfectly spherical flow of event energy, this ratio equals 0; for a perfectly jetty event, this ratio equals 1.0. For our electron tags, we require this ratio to be greater than 0.35. This final requirement helps remove contamination from semileptonic  $B$ -decays in  $B\bar{B}$  events. (The correlation between the soft pion momentum vector and the thrust axis is absent in  $B\bar{B}$  events, therefore  $B\bar{B}$  events do not contribute to our soft pion-tagged event sample.)

## III. TAG IDENTIFICATION

### A. Charm Tags

For our analysis, we select continuum hadronic events which, in addition to an antiproton, contain either a high momentum electron (from  $\bar{D} \rightarrow X e \nu$ ), a  $\pi_{\text{soft}}^-$  (from  $D^{*-} \rightarrow \bar{D}^0 \pi_{\text{soft}}^-$ ), or a fully reconstructed  $\bar{D}$ -meson candidate as a charm tag (“ $\bar{D}$ ”) of  $e^+e^- \rightarrow c\bar{c}$  events. Since the different tags have different systematic uncertainties and procedures associated with them, we now discuss separately the various tags employed in this measurement, beginning with our electron charm tags.

#### 1. Electron Tags

To suppress background from fake electrons, as well as true electrons not necessarily associated with charm decays in  $e^+e^- \rightarrow c\bar{c}$  events, we require that our electron-tag candidates satisfy the following criteria:

(a) The electron must pass a strict “probability of electron” identification criterion. This identification likelihood combines measurements of a given track’s specific ionization deposition in the central drift chamber with the ratio of the energy of the associated calorimeter shower to the charged track’s momentum [11]. True electrons have shower energies approximately equal to their drift chamber momenta; hadrons tend to be minimum ionizing and have considerably smaller values

of shower energy relative to their measured momenta. We require that the logarithm of the ratio of a charged track’s electron probability relative to the probability that the charged track is a hadron be greater than 7.0. In the good fiducial volume of the CLEO detector ( $|\cos\theta| < 0.7$ , where  $\theta$  is the track’s polar angle measured relative to the  $e^+e^-$  beam axis), the efficiency of this requirement is  $>90\%$  in our momentum interval of interest; the likelihood of a non-electron faking an electron is less than 1%. The total electron fake fraction is thus the product of the fake rate per track times the typical charged track multiplicity and is therefore not large ( $\leq 10\%$ ).

(b) The momentum of the electron must be greater than 1 GeV/ $c$ . This criterion helps eliminate fake electrons due to kaon and pion tracks and also suppresses electrons from photon conversions ( $\gamma \rightarrow e^+e^-$ ) and  $\pi^0$  Dalitz decays ( $\pi^0 \rightarrow \gamma e^+e^-$ ).

(c) The electron must have an impact parameter (“DOCA”, or distance-of-closest-approach) relative to the primary event vertex of less than 4 mm along the radial coordinate and no more than 2 cm along the beam axis. This provides additional suppression of electrons resulting from photon conversions.

## 2. Soft-pion Tags

Our soft-pion tag candidates must pass the following restrictions:

(a) The pion must have an impact parameter relative to the event vertex of less than 5 mm along the radial coordinate and no more than 5 cm along the beam axis.

(b) The pion must pass a 99% probability criterion for pion identification, based on the associated specific ionization collected in the drift chamber.

(c) The pion’s momentum must lie between 0.15 GeV/ $c$  and 0.40 GeV/ $c$ .

(d) The pion’s trajectory must lie near the trajectory of the parent charm quark, as expected for pions produced in  $D^{*-} \rightarrow \bar{D}^0 \pi_{\text{soft}}^-$ . Experimentally, this is checked using the variable  $\sin^2\theta$ , where  $\theta$  is the opening angle between the candidate soft pion and the event thrust axis [12]. Assuming that the thrust axis approximates the original  $c\bar{c}$  axis, true  $\pi_{\text{soft}}^-$  should populate the region  $\sin^2\theta \rightarrow 0$ . Fig. 1 displays the soft pion  $\sin^2\theta$  distribution for candidates passing our event and track selection criteria. The excess in the region  $\sin^2\theta \rightarrow 0$  constitutes our charm-tagged sample.

## 3. $\bar{D}^0$ , $D^-$ , and $D_s^-$ Tags

Fully reconstructed  $\bar{D}$ -meson tags are detected in the modes  $\bar{D}^0 \rightarrow K^+\pi^-$ ,  $D^- \rightarrow K^+\pi^-\pi^-$ , and  $D_s^- \rightarrow \phi\pi^-$ . In all cases, final state particles are required to pass DOCA criteria with respect to the primary vertex in both the radial ( $|\text{DOCA}| < 5$  mm) and beam ( $|\text{DOCA}| < 5$  cm) coordinates. Final state particles are also required to have specific ionization and time of flight information consistent with their assumed identities.

## B. Antiproton Tags

To be considered as candidates for antiproton (or proton, in the charge conjugate case) “tags”, charged particles detected in the central drift chamber must also pass strict particle identification criteria. Using the available time-of-flight and drift chamber specific ionization measurements for each track, the likelihood that a particle be an antiproton must be at least nine times larger than the likelihood that the particle be a  $K^-$  or a  $\pi^-$ . Antiproton tag candidates must also pass the

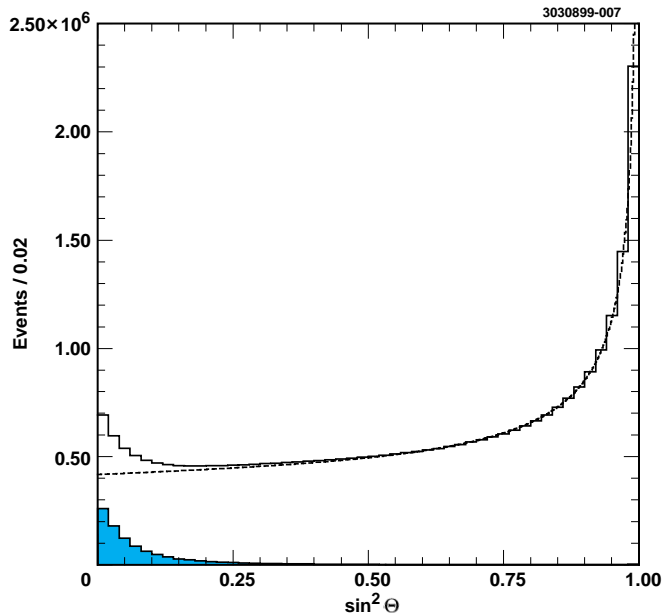


FIG. 1. Shown is the inclusive  $\sin^2\theta$  distribution for all tracks (solid histogram) overlaid with the background fit function (dashed) and the  $\pi_{\text{soft}}^-$  signal expected from  $D^{*-} \rightarrow \bar{D}^0 \pi_{\text{soft}}^-$  decays (shaded). Determination of signal and background follows an earlier CLEO analysis[12], which used this method to measure  $\mathcal{B}(D^0 \rightarrow K^- \pi^+)$ .

same vertex requirements as soft pion and electron candidates. These vertex criteria help suppress backgrounds from non-primary antiprotons (from  $\bar{\Lambda} \rightarrow \bar{p}\pi^+$ , e.g.) or baryons generated by collisions of beam particles with either the beampipe itself or residual gas within the beampipe.

It is important that our antiproton tags be direct, and not hyperon daughters. By combining our antiproton candidates with remaining charged tracks in the same event (assumed to be pions), we can reconstruct  $\bar{\Lambda}$ 's and estimate the fraction of our antiproton tags which are due to reconstructed  $\bar{\Lambda}$ 's decay. We determine this fraction to be  $<2\%$  (Sect. IV A 3).

We check the fraction of our proton tags originating in beam-gas and beam-wall collisions by determining the asymmetry between the number of proton tags and antiproton tags. If the beam-gas/beam-wall contamination is large, we expect there to be a preponderance of proton tags compared to antiproton tags. In fact, in a  $\bar{D}$ -meson tagged subset of the full data used in this analysis, we find the number of proton tags ( $6980 \pm 255$ ) to be statistically equal to the number of antiproton tags ( $6737 \pm 250$ ). Nevertheless, the difference between these two numbers is taken as our systematic uncertainty in the magnitude of beam-related backgrounds (Table II).

#### IV. TRIPLE CORRELATIONS

In the triple correlation analysis, we tag the  $\bar{c}$  side of an  $e^+e^- \rightarrow c\bar{c}$  event using a soft pion or an electron tag, then search for a  $\bar{p}$  in the opposite hemisphere. In order to conserve both charm and baryon number we assume a  $\Lambda_c^+$  in the hemisphere opposite the tag. Below we show a schematic diagram of an event where either a  $\pi_{\text{soft}}^-$  or  $e^-$ , in combination with an anti-proton, is used to tag an unseen ( $\Lambda_c^+$ ) decay.



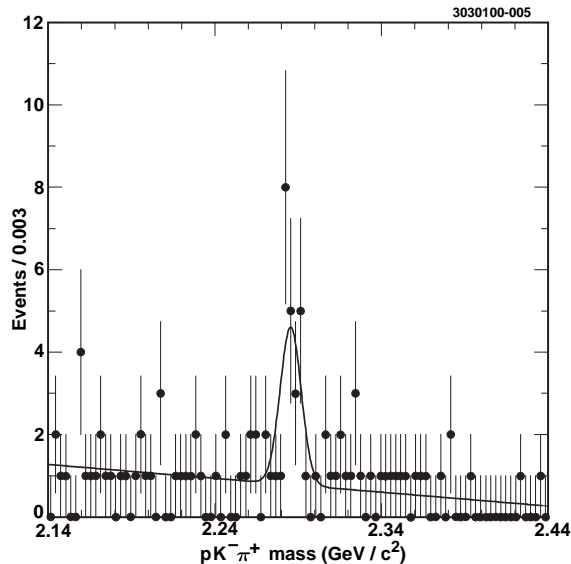


FIG. 2. The candidate  $\Lambda_c^+$  mass (i.e.,  $pK^-\pi^+$  mass, in  $\text{GeV}/c^2$ ) for  $\Lambda_c^+$ 's with a  $\bar{p}$  in the same hemisphere [ $\Lambda_c^+\bar{p}$ ] and an  $e^-$  in the opposite hemisphere ( $\Lambda_c^+e^-$ ). The triple correlation yield is  $10.3 \pm 3.8$  events.

$$\begin{array}{ccccccc}
 & & & c \bar{c} & & & \\
 & & & \swarrow & \searrow & & \\
 \bar{p} \leftarrow & & & & \leftrightarrow D^{*-} & & \\
 (\Lambda_c^+) \leftarrow & & & & \leftrightarrow \bar{D}^0 \pi_{\text{soft}}^- & & \\
 (\text{anything}) \leftarrow & & & & \leftrightarrow e^- K^+ \nu_e & & 
 \end{array}$$

The above diagram gives us a known sample of  $\Lambda_c^+$  events. (Note that we do not require that both  $\pi_{\text{soft}}^-$  and  $e^-$  tags be present in a candidate event; the presence of either one constitutes a valid “charm-tag”.) In the electron tag case, the total number of  $\Lambda_c^+$ 's is the number of events in which a track passes our electron tag identification and an antiproton tag is found in the opposite hemisphere. We then reconstruct, in that sample, a  $\Lambda_c^+$  decaying into  $pK^-\pi^+$  in the same hemisphere as the  $\bar{p}$ , and opposite the electron candidate. The  $\Lambda_c^+$  invariant mass distribution is then fit to a first order Chebyshev Polynomial to represent the background and a Gaussian to represent the signal (Fig. 2), with the  $\Lambda_c^+$  mass and width fixed to the values obtained from a fit to the inclusive  $\Lambda_c^+$  mass spectrum in data.

When using the soft pion tag, we select events that are supposed to contain a  $\Lambda_c^+$  by plotting the  $\sin^2\theta$  distribution of pions with a tag  $\bar{p}$  in the opposite hemisphere, with  $\theta$  defined as before as the angle between the pion's momentum and the thrust axis (Fig. 1). Background and signal distributions are then fit to this  $\sin^2\theta$  distribution. The background function we use is  $f(x) = C_1(1/\sqrt{1-x}) + C_2(1/\sqrt{1+Ax^2+Bx^3})$ , where  $x$  is  $\sin^2\theta$ . This functional form is taken from a previous CLEO measurement of  $\mathcal{B}(D^0 \rightarrow K^-\pi^+)$  using a similar technique [13].

Using the soft pion tag, we extract the number of signal events from a two-dimensional plot of  $pK^-\pi^+$  invariant mass versus the  $\sin^2\theta$  of the  $\pi_{\text{soft}}^-$ . From this two-dimensional distribution, we

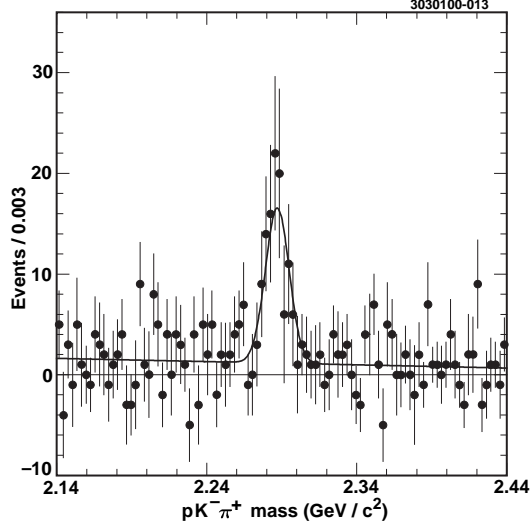


FIG. 3. Results of sideband subtraction in data to determine  $\Lambda_c^+ \rightarrow pK^-\pi^+$  yield in soft-pion tagged events. We project onto the candidate  $\Lambda_c^+$  mass axis the portion of our two-dimensional  $pK^-\pi^+$  mass vs.  $\sin^2\theta$  plot corresponding to  $\sin^2\theta < 0.25$  and subtract the scaled projection corresponding to  $0.25 \leq \sin^2\theta \leq 0.5$ . We then perform a fit to the resulting  $pK^-\pi^+$  mass spectrum in order to find our final yield of  $c\bar{c} \rightarrow \Lambda_c^+ + \bar{p} + \pi_{\text{soft}}^- + X$  events. The raw triple correlation yield is  $101.6 \pm 20.6$  events.

perform a scaled sideband subtraction of the  $\Lambda_c^+$  yield in the “sideband” region ( $0.25 < \sin^2\theta < 0.5$ ) compared with the signal region ( $\sin^2\theta < 0.25$ ) to determine the final, background-subtracted yield (Fig. 3). (The background is approximately linear through this region.) We have compared the yield obtained this way with the yield obtained using the  $\sin^2\theta$  signal remaining after  $\Lambda_c^+$ -mass sideband subtraction ( $91 \pm 18$  events). The two techniques give consistent results; the difference between them is counted towards the final systematic error (Table II).

For both tags, we can now quantify the ratio of tagged events containing a  $\Lambda_c^+$  decaying into  $pK^-\pi^+$  to all tagged events. This ratio is equal to

$$R = \frac{\mathcal{Y}(e^+e^- \rightarrow \bar{D} + \bar{p} + (\Lambda_c^+ \rightarrow pK^-\pi^+) + X)}{\mathcal{Y}(e^+e^- \rightarrow \bar{D} + \bar{p} + X)} \quad (1)$$

where  $\mathcal{Y}$  stands for “yield in  $e^+e^-$  annihilation”, “ $\bar{D}$ ” designates any one of our charm tags, and the  $\bar{p}$  and the  $\bar{D}$  are in opposite hemispheres with respect to the thrust axis of the event.

Now the numerator can be written as

$$\begin{aligned} &\mathcal{Y}(e^+e^- \rightarrow \bar{D} + \bar{p} + (\Lambda_c^+ \rightarrow pK^-\pi^+) + X) = \\ &\mathcal{L} \cdot \sigma(e^+e^- \rightarrow c\bar{c}) \cdot \mathcal{B}(c\bar{c} \rightarrow \bar{D} + \bar{p} + \Lambda_c^+ + X) \cdot \mathcal{B}(\Lambda_c^+ \rightarrow pK^-\pi^+) \cdot (\epsilon_{\bar{D}}) \cdot (\epsilon_{\bar{p}}) \cdot (\epsilon_{\Lambda_c^+}) \end{aligned} \quad (2)$$

and the denominator

$$\mathcal{Y}(e^+e^- \rightarrow \bar{D} + \bar{p} + X) = \mathcal{L} \cdot \sigma(e^+e^- \rightarrow c\bar{c}) \cdot \mathcal{B}(c\bar{c} \rightarrow \bar{D} + \bar{p} + \Theta_c + X') \cdot (\epsilon_{\bar{D}}) \cdot (\epsilon_{\bar{p}}) \quad (3)$$

where  $\Theta_c$  is any charm+baryon system, not necessarily a  $\Lambda_c^+$  (e.g. it could be a  $D$  + nucleon or a charmed baryon, such as a  $\Xi_c$ , not always decaying into  $\Lambda_c^+ + X$ ),  $\mathcal{L}$  is the total luminosity, and  $\epsilon_{\bar{p}}$ ,  $\epsilon_{\Lambda_c^+}$ , and  $\epsilon_{\bar{D}}$  are the efficiencies of finding the antiproton,  $\Lambda_c^+$ , and charm tags, respectively.

We then write

$$\mathcal{Y}(e^+e^- \rightarrow \bar{D} + \bar{p} + X) = f_1 \cdot \mathcal{L} \cdot \sigma(e^+e^- \rightarrow c\bar{c}) \cdot \mathcal{B}(c\bar{c} \rightarrow \bar{D} + \bar{p} + \Lambda_c^+ + X) \cdot \epsilon_{\bar{D}} \cdot \epsilon_{\bar{p}} \quad (4)$$

where

$$f_1 \equiv \frac{\mathcal{B}(c\bar{c} \rightarrow \bar{D} + \bar{p} + \Theta_c + X')}{\mathcal{B}(c\bar{c} \rightarrow \bar{D} + \bar{p} + \Lambda_c^+ + X)}. \quad (5)$$

Since  $f_1$  takes into account the fact that our yield includes also charmed, baryonic systems other than  $\Lambda_c$ ,  $f_1 \geq 1.0$ . Then:

$$\mathcal{B}(\Lambda_c^+ \rightarrow pK^-\pi^+) = \frac{R \cdot f_1}{\epsilon_{\Lambda_c^+}}. \quad (6)$$

Since the above equation holds for both data and Monte Carlo simulations we can write:

$$\frac{\mathcal{B}(\Lambda_c^+ \rightarrow pK^-\pi^+)_{Data}}{\mathcal{B}(\Lambda_c^+ \rightarrow pK^-\pi^+)_{MC}} = \frac{R_{Data} \cdot \epsilon_{\Lambda_c^+}(MC) \cdot f_1(Data)}{R_{MC} \cdot \epsilon_{\Lambda_c^+}(Data) \cdot f_1(MC)}. \quad (7)$$

We use Monte Carlo simulations to determine event and particle reconstruction efficiencies. The simulated sample size corresponds to approximately  $6 \text{ fb}^{-1}$  of integrated luminosity. Our Monte Carlo simulation combines an  $e^+e^- \rightarrow c\bar{c}$  event generator (JETSET 7.3 [14]) with a GEANT-based [15] simulation of our detector. Assuming that the detector simulation accurately reproduces the efficiency of reconstructing a  $\Lambda_c^+$  in a tagged event and that we can determine the correction  $f_1$  in both data and Monte Carlo, we can then calibrate our observed value of  $\Lambda_c^+$  per tagged event in data to Monte Carlo:

$$\frac{f_{1,Data}}{f_{1,MC}} \frac{R_{Data}}{R_{MC}} \cdot \mathcal{B}(\Lambda_c^+ \rightarrow pK^-\pi^+)_{MC} = \mathcal{B}(\Lambda_c^+ \rightarrow pK^-\pi^+)_{Data}. \quad (8)$$

## A. Purity of Our Event Sample

We seek, wherever possible, to measure backgrounds directly from data and thereby minimize the Monte Carlo dependence; i.e., we prefer to measure  $f_{1(Data)}$  and  $f_{1(MC)}$  separately rather than to assume equality of these fractions. According to event simulations, the primary non- $\Lambda_c^+$  contribution to the numerator of  $f_1$  is due to events where baryon number opposite the  $\bar{p}$  tag is conserved by another nucleon and a  $D$  meson is created in the hemisphere opposite our anticharm (“ $\bar{D}$ ”) tag, so that no  $\Lambda_c^+$  is present in the event. We refer to these events as  $D\bar{D}N\bar{p}$  events. In order to estimate the number of  $D\bar{D}N\bar{p}$  events that contaminate our tagged event sample, we measure the number of events containing a  $\bar{p}$  tag and a  $D$  meson in the same hemisphere ( $S[\bar{p}D]$ , see Figure 4) and assume (without reconstructing) a  $\bar{D}$  in the opposite hemisphere to conserve charm. A correction ( $11\pm 2\%$  in data, described in Sections (IV A) and (V B 1) of this document) is made to  $\mathcal{B}(\Lambda_c^+ \rightarrow pK^-\pi^+)$  based on the observed yields of these  $D\bar{D}N\bar{p}$  events in data and Monte Carlo. A much smaller contribution to  $f_1$  arises from  $\Xi_c X\bar{D}\bar{p}$  (also discussed later in the text).

Anti-protons from  $\bar{\Lambda}_c$  decay entering the hemisphere of the  $D$  meson and  $\bar{\Lambda}_c\bar{p}D$  events must not be large in order for our assumption that the  $S[D\bar{p}]$  sample can be used to estimate the level of  $D\bar{D}N\bar{p}$  background be valid. In order to check for anti-protons from  $\bar{\Lambda}_c$ ’s decaying into the hemisphere of a  $D$  we plot the cosine of the angle between the anti-proton’s momentum vector and its parent  $\bar{\Lambda}_c$ . For anti-protons passing our event and track criteria, back hemisphere leakage is found to be negligible ( $< 1\%$ ). Events containing  $\bar{\Lambda}_c\bar{p}D$  must contain two baryon-anti-baryon pairs as well as a charmed meson (e.g.  $\bar{\Lambda}_c\bar{p}NND$ ). Although it is possible to have four baryons and a charmed meson in the same event it should be noted that this process would lead to an overestimation of our background (i.e. events that contain a  $D\bar{p}$  but do not tag  $D\bar{D}N\bar{p}$  events), thus biasing us towards a  $\mathcal{B}(\Lambda_c^+ \rightarrow pK^-\pi^+)$  that is higher than the true branching fraction. Monte Carlo simulations indicate that this background is exceedingly ( $< 1\%$ ) small.

### 1. Contamination of the $\pi_{\text{soft}}^-$ sample

Pions from  $\Sigma_c^0 \rightarrow \Lambda_c^+\pi^-$  and orbitally excited  $\Lambda_{cJ}^+ \rightarrow \Lambda_c^+\pi^+\pi^-$  decays have  $\sin^2\theta$  distributions similar to the soft pions from  $D^{*-}$  decays as seen in Figure 5. Although the number of  $\Sigma_c^0$  and  $\Lambda_{cJ}^-$  particles (primarily  $\Lambda_c^-(2593)$  and  $\Lambda_c^-(2630)$ ) is small relative to the number of  $D^{*-}$  particles, this background is potentially significant since the likelihood for having a  $\bar{p}$  tag is large in events containing these charmed baryons. In order to estimate the magnitude of these events in data and Monte Carlo we perform a fit using Monte Carlo-derived  $\sin^2\theta$  distributions for tagged  $\pi_{\text{soft}}^-$  decaying from both  $D^{*-}$  and  $\Sigma_c^0$  decays. We fit these distributions to our plot of the inclusive  $\pi_{\text{soft}}^-$   $\sin^2\theta$  spectrum in events containing a  $\bar{p}$  in the hemisphere opposite the  $\pi_{\text{soft}}^-$  with respect to the thrust axis (see Figure 6). The difference between the data and Monte Carlo ( $\Sigma_c + \Lambda_{c,J}$ )  $\pi_{\text{soft}}^-$  fit fractions relative to the total  $\pi_{\text{soft}}^-$  yield in data ( $14 \pm 17\%$ ) as compared to Monte Carlo ( $21 \pm 9\%$ )<sup>‡‡</sup> is taken as a systematic error (Table II).

---

<sup>‡‡</sup>The actual fraction in Monte Carlo is 12%.

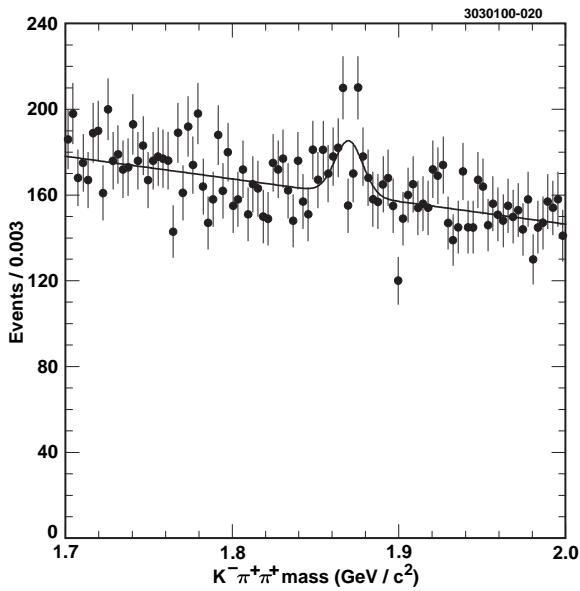
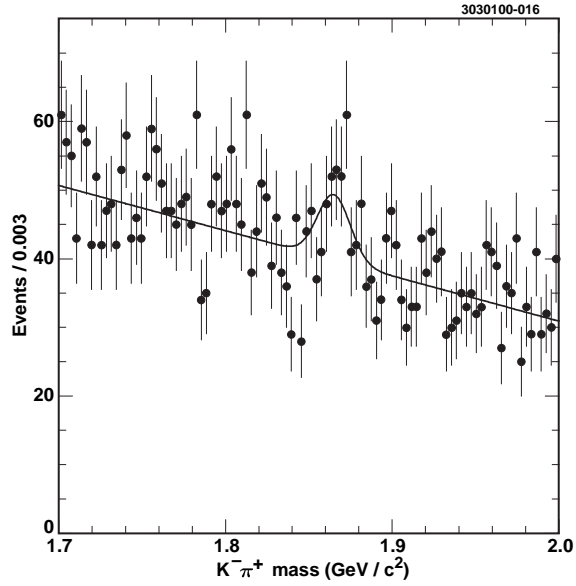


FIG. 4. Candidate  $D^0$  (top) and  $D^+$  (bottom) mass ( $\text{GeV}/c^2$ ) for  $D$  candidates in the same hemisphere as a  $\bar{p}$  [ $D\bar{p}$ ]. Events in the  $D$  signal region are  $D\bar{D}N\bar{p}$  events that contaminate our candidate  $\Lambda_c^+$  event sample. The masses and widths of the  $D^0$  and  $D^+$  are taken from fits to the inclusive mass spectra in data.

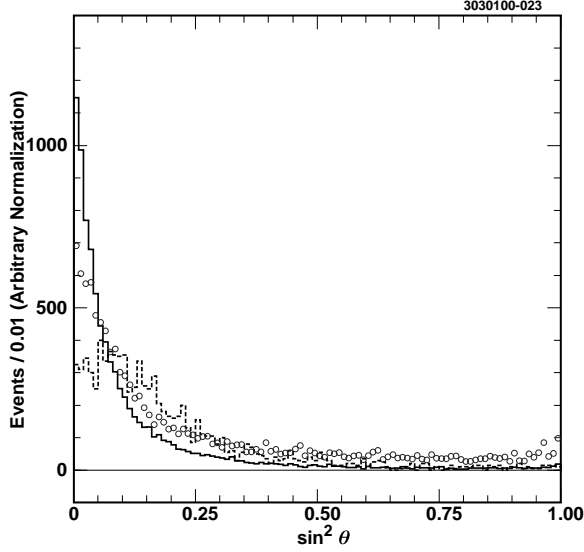


FIG. 5. Monte Carlo  $\sin^2\theta$  distribution of  $\pi^-$ 's from  $D^{*-} \rightarrow D^0\pi^-$  (solid line),  $\Lambda_{cJ}^+(2593) \rightarrow \Lambda_c^+\pi^+\pi^-$  (diamonds), and  $\Sigma_c^0 \rightarrow \Lambda_c^+\pi^-$  (dashed line) after all event and particle identification cuts are applied to the  $\pi^-$ 's.

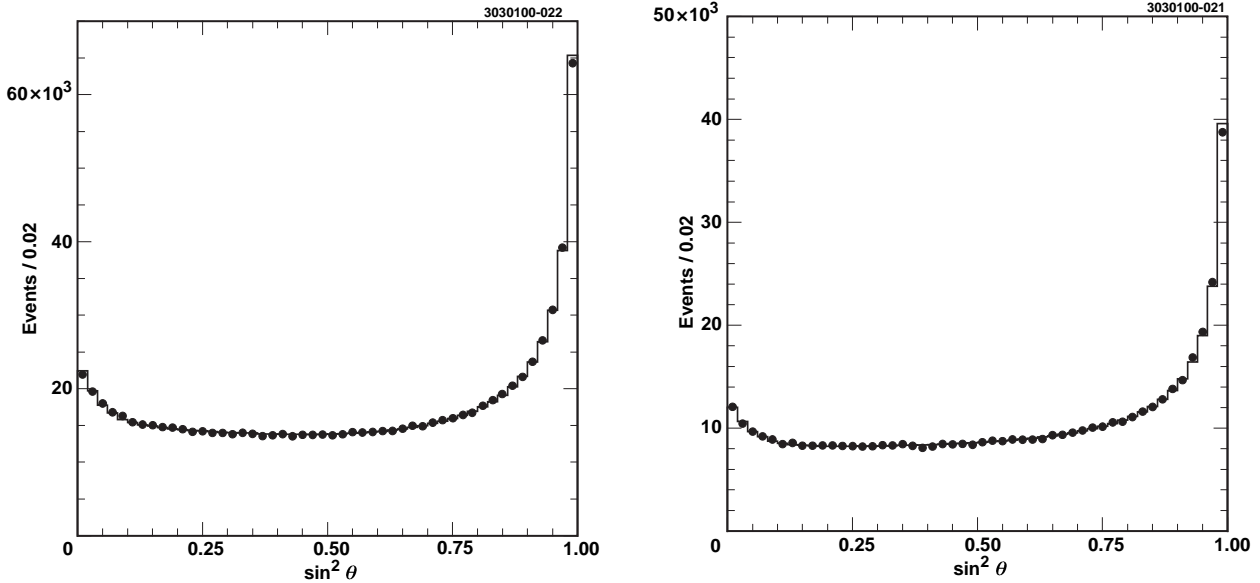


FIG. 6.  $\sin^2\theta$  distribution of  $\pi^-$ 's in data events containing a tag antiproton in the opposite hemisphere  $O(\pi_{\text{soft}}^-|\bar{p})$ , for Monte Carlo simulations (left) vs. data (right). A free fit is performed using the Monte Carlo  $\sin^2\theta$  distributions for  $\pi^-$ 's decaying from  $D^{*-} \rightarrow D^0\pi^-$ ,  $\Sigma_c^0 \rightarrow \Lambda_c^+\pi^-$ , and  $\Lambda_c(2593) \rightarrow \Lambda_c^+\pi^+\pi^-$ . This plot is made after all event and  $\pi_{\text{soft}}^-$  particle identification cuts have been applied. The fitted  $\Sigma_c + \Lambda_{cJ}$  fractions for Monte Carlo and data are  $21 \pm 9\%$  and  $14 \pm 17\%$ , respectively.

## 2. Electron Tag Backgrounds

We assume that our tag electrons are not only true electrons in  $c\bar{c}$  events, but also that they are coming from semileptonic charm decay. In Monte Carlo,  $\sim 87\%$  of our tag electrons are true electrons coming from charm semileptonic decays. The remainder of our tag electrons are either background fakes (i.e., non-electrons) or background electrons not from charm decays (predominantly from the decay  $\pi^0 \rightarrow e^+e^-\gamma$ ). Each of these backgrounds contributes approximately equally to our candidate electron sample. The number of fake electron tags should cancel in our equation for  $\mathcal{B}(\Lambda_c^+ \rightarrow pK^-\pi^+)$ , unless there is a decreased probability of tag electron fakes in events that contain a  $\Lambda_c^+\bar{p}$  as compared to those only containing a  $\bar{p}$ . Since this very well may be the case, we vary the electron identification cuts and take the change in the calculated  $\mathcal{B}(\Lambda_c^+ \rightarrow pK^-\pi^+)$  as a systematic error (5%, as listed in Table II).

Another possible source of tag electron background is from two-photon annihilations, in which one of the incident beam particles scatters into the detector. The two-photon contamination is assessed by determining the asymmetry between the number of positrons in the forward hemisphere compared to the number of electrons in the negative hemisphere (beam positrons define  $+\hat{z}$  in the local coordinate system). We find two-photon annihilations to be negligible ( $< 1\%$ ) in our tag electron sample.

## 3. Backgrounds from $([\Xi_c\bar{\Lambda}]\bar{D})$

Tagged events may also contain a charmed baryon other than a  $\Lambda_c^+$ ; most likely a  $\Xi_c$ . It is therefore important to check that the ratio of  $\Xi_c/\Lambda_c^+$  production rates is similar in data and Monte Carlo simulations. Monte Carlo simulations (JETSET 7.3) indicate that, in events passing our event selection criteria, and having an antiproton tag originating from the primary vertex,  $\Xi_c/\Lambda_c^+=0.014$ . Since this fraction is so small in Monte Carlo simulations, the data fraction must be inconsistent with the Monte Carlo expectation by at least an order of magnitude to make a significant difference in our calculation of  $\mathcal{B}(\Lambda_c^+ \rightarrow pK^-\pi^+)$ . In order to check the fraction of our tagged event sample containing a  $\Xi_c$  instead of a  $\Lambda_c^+$ , we plot the  $\sin^2\theta$  of  $\pi_{\text{soft}}^-$  versus the mass of an opposite hemisphere  $\bar{\Lambda}$  (Figure 7), rather than an opposite hemisphere  $\bar{p}$ . This is not the correct sign correlation for  $\Xi_c \rightarrow \bar{\Lambda}$  decays since the  $\pi_{\text{soft}}^-$  tags a  $D^{*-}$  (such a correlation implies  $\bar{c}$  in both hemispheres). Instead, we assume that the dominant contributor to this plot is from  $\bar{\Lambda}$ 's conserving baryon number with a same hemisphere  $\Xi_c$  (i.e.  $([\Xi_c\bar{\Lambda}]D^{*-})X$  events). Although other  $O(\bar{\Lambda}\bar{D})$  topologies may contribute (e.g.  $\bar{D}^0\bar{\Lambda}K^-N$ ), it is still probable that an excess of  $\Xi_c$  production in our  $\pi_{\text{soft}}^-$  event sample would be noticed as an excess in  $\bar{\Lambda}$  production opposite our tag  $\pi_{\text{soft}}^-$ . In fact we do not see this excess; we find  $(1.3 \pm 0.2) \times 10^{-3}$   $\bar{\Lambda}$  per  $\pi_{\text{soft}}^-$  tagged event in data vs.  $(1.6 \pm 0.2) \times 10^{-3}$  in Monte Carlo simulations. (Note that we have already suppressed  $\Xi_c\bar{\Lambda}D^{*-}$  events by requiring the tag anti-proton to come from the primary event vertex.) These checks do not however address a possible excess of  $\Xi_c\bar{p}KD^{*-}$  events. In principle one could estimate  $\Xi_c/\Lambda_c$  in data by reconstructing  $\Xi_c$ 's in the hemisphere of a tag anti-proton. However, we are unable to make an accurate estimate of the  $\Xi_c\bar{p}$  yield due to low reconstruction efficiency. Therefore, using the similarity of the relative  $\bar{\Lambda}/\pi_{\text{soft}}^-$  production ratio in data vs. Monte Carlo simulations as guidance, we assume the same  $\Xi_c/\Lambda_c$  production ratio in data as in Monte Carlo simulations. It should be noted that although the systematic error assessed due to uncertainties in  $\Xi_c$  production is small (3%, see Table II), this magnitude of systematic error represents twice the amount of  $\Xi_c$  production predicted by Monte Carlo simulations for our tagged event sample.

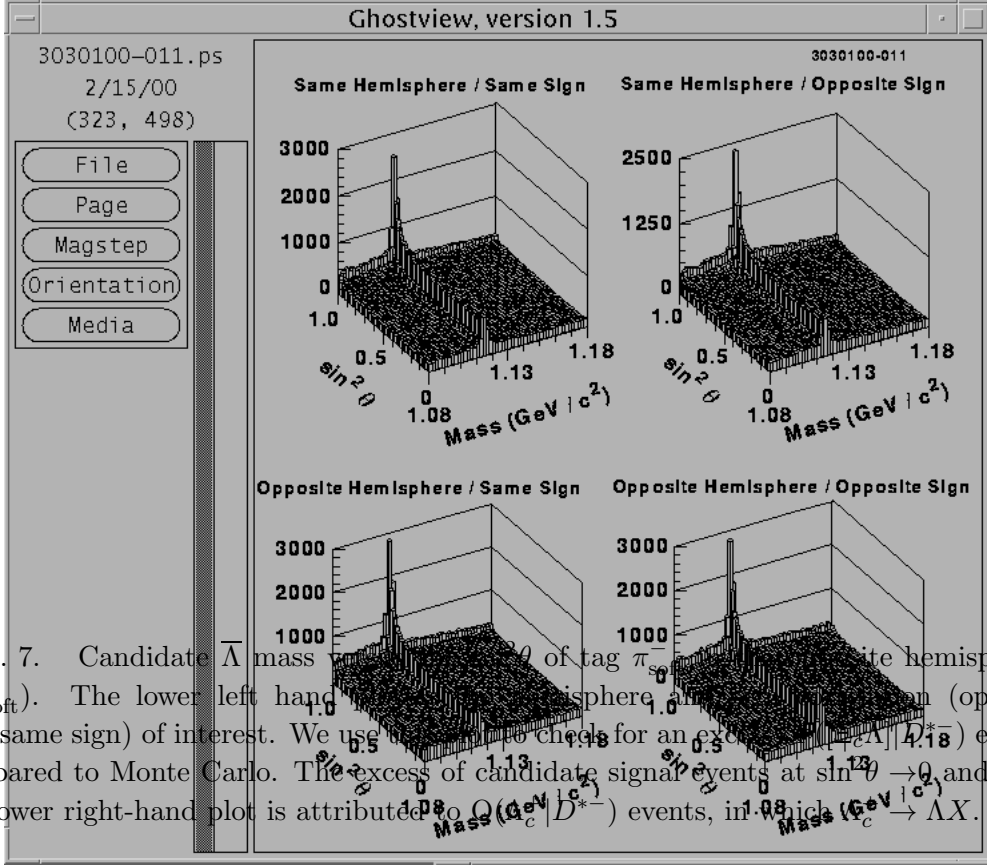


FIG. 7. Candidate  $\bar{\Lambda}$  mass vs.  $\sin^2 \theta$  of tag  $\pi_{\text{soft}}^-$  in data (opposite hemisphere in data  $O(\bar{\Lambda}|\pi_{\text{soft}}^-)$ ). The lower left hand plot is same hemisphere/same sign (opposite hemisphere/opposite sign) of interest. We use the other two plots to check for an excess of candidate signal events as compared to Monte Carlo. The excess of candidate signal events at  $\sin^2 \theta \rightarrow 0$ , and  $m_{\pi^-} \sim m_{\Lambda}$  in the lower right-hand plot is attributed to  $D^0 \rightarrow \bar{c}c D^{*-}$  events, in which  $\bar{c} \rightarrow \bar{\Lambda} X$ .

## B. Hemisphere Correlation

There is an additional systematic error due to the hemisphere correlation requirements we impose on the  $(\bar{p}|\bar{D})$  and  $(\bar{p}|\Lambda_c^+)$  samples. In fact, not all  $\bar{p}\bar{D}\Lambda_c^+$  events in which the  $\bar{p}\bar{D}$  are in opposite hemispheres necessarily have the  $\bar{p}\Lambda_c^+$  in the same hemisphere (e.g., if the three momentum vectors have opening angles of  $120^\circ$  between them). This can happen in events with photon or gluon radiation. For  $c\bar{c}g$  or  $c\bar{c}\gamma$  (initial state radiation) events, the  $c\bar{c}$  will not be directly back to back. This can be seen in Figure 8, which shows the  $\bar{p}\bar{D}$  opening angle vs. the  $\bar{p}\Lambda_c^+$  opening angle for Monte Carlo  $\bar{p}\bar{D}\Lambda_c^+$  events. Note that, in producing this distribution, we have not required that either the  $\bar{D}$  or  $\Lambda_c^+$  be high momentum, as we would for our standard data analysis, whereas the momenta for charm particles in radiative  $c\bar{c}$  events is typically smaller. Nevertheless, the fraction of  $\Lambda_c^+\bar{p}\bar{D}$  events in which the antiproton is found in the lower-left quadrant of Figure 8 is taken as a systematic error (Table II), reflecting the fact that the hemisphere correlation is not rigorous, and that these angular distributions may be different in data vs. Monte Carlo.

## V. DOUBLE CORRELATIONS

### A. Method

In order to circumvent the low statistics involved with the triple correlation methods we exploit a double correlation method. We begin with events containing a  $S[\bar{p}\Lambda_c^+]$  in the same hemisphere.



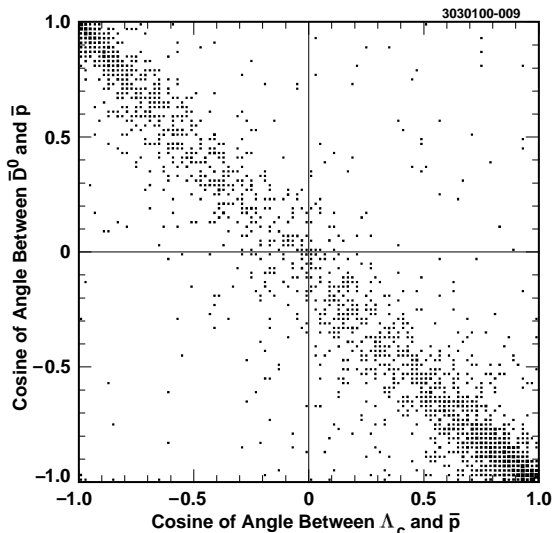


FIG. 8. Cosine of the angle between the tag anti-proton momentum vector and  $\Lambda_c^+$  momentum vector (horizontal) versus cosine of the angle between the tag anti-proton momentum and  $\overline{D}^0$  momentum (vertical) in  $\Lambda_c^+ \overline{D}^0 \overline{p}$  events from Monte Carlo simulations, with no particle cuts (i.e., minimum momentum and track reconstruction cuts, etc.) applied. Events in the lower-left hand quadrant are due primarily to  $c\overline{c}g$  and  $c\overline{c}\gamma$  events. In these events we have an antiproton that passes our tag anti-proton cuts but is in the opposite hemisphere of both a  $\Lambda_c^+$  and a  $\overline{D}^0$ , thus giving us a slight excess ( $\sim 2\%$ ) of  $\overline{D}^0$  opposite  $\overline{p}$  events relative to  $\Lambda_c^+ \overline{p}$  same hemisphere events. The lower-right hand quadrant corresponds to our signal events. The upper-left hand quadrant event sample is used later for a cross-check (Sect VD).

In these events a  $\bar{c}$ -hadron can be assumed in the hemisphere opposite the  $\Lambda_c^+$ . This  $\bar{c}$ -hadron will most likely be an anti-charmed meson. Events containing an anti-charmed baryon opposite a  $\bar{p}\Lambda_c^+$  should be suppressed due to the energy required to create four baryons in an event, as well as the small  $c \rightarrow \Lambda_c$  fragmentation rate. Below is a representation of a sample event in which a  $\bar{p}$  and a  $\Lambda_c^+ \rightarrow pK^-\pi^+$  are observed with a  $\bar{D}^0$  or  $D^-$  or  $D_s^-$  assumed to exist in the opposite hemisphere.

$$\begin{array}{ccc}
& c \bar{c} & \\
\bar{p} \leftrightarrow & \leftrightarrow (\bar{D}^0 \text{ or } D^- \text{ or } D_s^-) & \\
\Lambda_c^+ \leftrightarrow & & \leftrightarrow \textit{anything} \\
pK^-\pi^+ \leftrightarrow & & 
\end{array}$$

After finding the number of  $S[\bar{p}\Lambda_c^+]$  events (Figure 9), we separately find the number of times that a  $\bar{p}$  is found opposite a  $\bar{D}$ . For this double correlation measurement, fully reconstructed mesons are used as the anticharm tag  $\bar{D}$ . We reconstruct the  $\bar{D}^0$  (Figure 10) through the  $K^+\pi^-$  decay mode, the  $D^-$  (Figure 11) through the  $K^+\pi^-\pi^-$  decay mode, and the  $D_s^-$  (Figure 12) through the  $\phi\pi^-$  decay mode. We require the  $\bar{D}$ -meson to have momentum  $p > 2.5$  GeV/ $c$ , beyond the maximum possible in  $B \rightarrow \bar{D}X$  events. In these events we assume a  $\Lambda_c^+$  in the hemisphere opposite the  $\bar{D}$ .

$$\begin{array}{ccc}
& c \bar{c} & \\
\bar{p} \leftrightarrow & \leftrightarrow \bar{D}^0 \text{ or } D^- \text{ or } D_s^- & \\
(\Lambda_c^+) \leftrightarrow & & \leftrightarrow K^+\pi^- \text{ or } K^+\pi^-\pi^- \text{ or } \phi\pi^- \\
\textit{anything} \leftrightarrow & & 
\end{array}$$

Comparing the number of  $S[\bar{p}\Lambda_c^+]$  events to the number of  $O(\bar{p}|\bar{D})$  events, we are able to calculate  $B(\Lambda_c^+ \rightarrow pK^-\pi^+)$ , as follows. First we write an equation for  $\mathcal{Y}(\Lambda_c^+)$ , the yield of  $\Lambda_c^+ \rightarrow pK^-\pi^+$  events containing a tag antiproton in the same hemisphere of the  $\Lambda_c^+$ :

$$\mathcal{Y}[\Lambda_c^+\bar{p}] = \frac{\mathcal{L} \cdot \sigma(e^+e^- \rightarrow c\bar{c}) \cdot \mathcal{B}(c\bar{c} \rightarrow \bar{p} + \Lambda_c^+ + X + \bar{D}^0 \text{ or } D^- \text{ or } D_s^-) \cdot \mathcal{B}(\Lambda_c^+ \rightarrow pK^-\pi^+) \cdot \epsilon_{\bar{p}} \cdot \epsilon_{[\Lambda_c^+\bar{p}]}}{1 - f_2}, \quad (9)$$

where  $\epsilon_{[\Lambda_c^+\bar{p}]}$  is the efficiency for reconstructing a  $\Lambda_c^+ \rightarrow pK^-\pi^+$  decay in an event containing a tag anti-proton and  $f_2$  is defined as the fraction of  $\Lambda_c^+\bar{p}$  events not containing a  $\bar{D}^0$  or  $D^-$  or  $D_s^-$ :

$$f_2 \equiv \frac{\mathcal{B}(c\bar{c} \rightarrow \bar{p} + \Lambda_c^+ + X' + \textit{anticharmed baryon})}{\mathcal{B}(c\bar{c} \rightarrow \bar{p} + \Lambda_c^+ + X)} \quad (10)$$

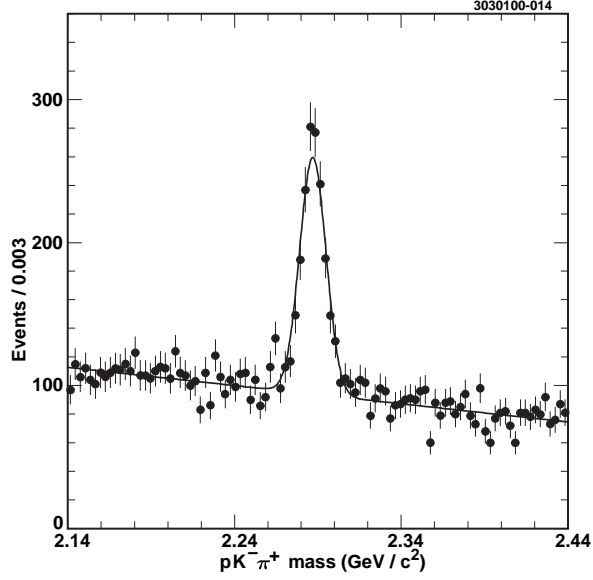


FIG. 9. Candidate  $\Lambda_c^+$  mass (i.e.,  $pK^-\pi^+$  mass, in  $\text{GeV}/c^2$ ) for  $\Lambda_c^+$ 's with a  $\bar{p}$  in the same hemisphere  $S[\bar{p}\Lambda_c^+]$ . In these events a  $\bar{D}$  meson is assumed to recoil in the hemisphere opposite the  $\Lambda_c^+$ :  $O(\bar{D}|\Lambda_c^+)$ .

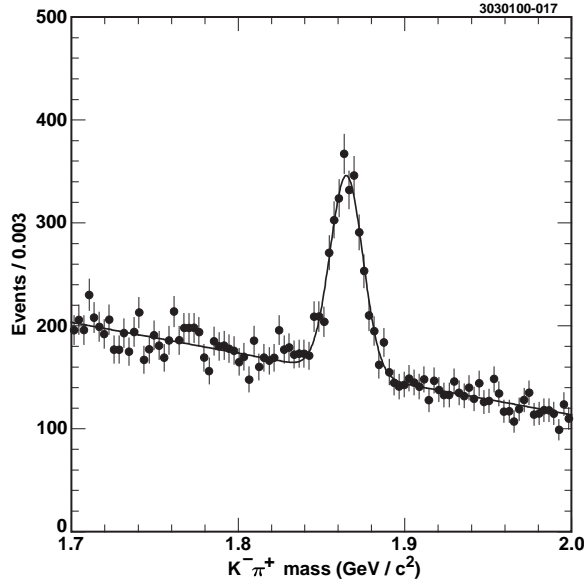


FIG. 10. Candidate  $\bar{D}^0$  mass (i.e.,  $K^+\pi^-$  mass, in  $\text{GeV}/c^2$ ) with a  $\bar{p}$  in the opposite hemisphere  $O(\bar{D}^0|\bar{p})$ . In these events a  $\Lambda_c^+$  is assumed to exist in the hemisphere opposite the  $\bar{D}^0$ :  $O(\bar{D}^0|\Lambda_c^+)$ .

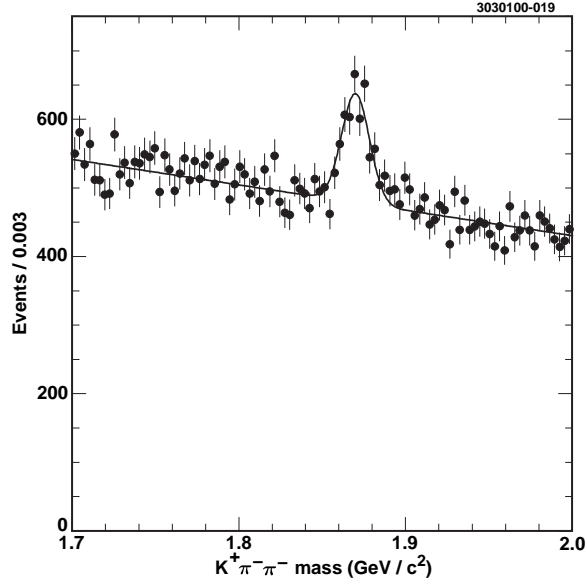


FIG. 11. Candidate  $D^-$  mass (i.e.,  $K^+\pi^-\pi^-$  mass, in  $\text{GeV}/c^2$ ) with a  $\bar{p}$  in the opposite hemisphere. In these events a  $\Lambda_c^+$  is assumed to exist in the hemisphere opposite the  $D^-$ :  $O(D^-|\Lambda_c^+)$ .

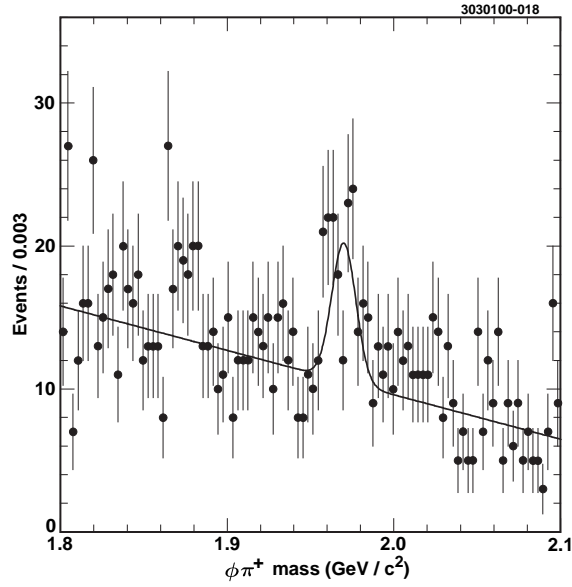


FIG. 12. Candidate  $D_s^-$  mass (i.e.,  $\phi\pi^-$  mass, in  $\text{GeV}/c^2$ ) with a  $\bar{p}$  in the opposite hemisphere. In these events a  $\Lambda_c^+$  is assumed to exist in the hemisphere opposite the  $D_s^-$ :  $O(D_s^-|\Lambda_c^+)$ .

where the anticharmed baryon could be, e.g. a  $\bar{\Lambda}_c$  in which case two baryon pairs must exist in the event.

For  $\mathcal{Y}(\bar{D}^0|\bar{p})$ , the yield of events containing a  $\bar{D}^0 \rightarrow K^+\pi^-$  decay in the hemisphere opposite a tag  $\bar{p}$ , one can write:

$$\mathcal{Y}(\bar{D}^0|\bar{p}) = \frac{\mathcal{L} \cdot \sigma(e^+e^- \rightarrow c\bar{c}) \cdot \mathcal{B}(c\bar{c} \rightarrow \bar{p} + \Lambda_c^+ + \bar{D}^0 + X) \cdot \mathcal{B}(\bar{D}^0 \rightarrow K^+\pi^-) \cdot \epsilon_{\bar{p}} \cdot \epsilon_{(\bar{D}^0|\bar{p})}}{1 - f_3} \quad (11)$$

and similarly for  $\mathcal{Y}(D^-)$  and  $\mathcal{Y}(D_s^-)$ , where  $\epsilon_{(\bar{D}^0|\bar{p})}$  is the efficiency for reconstructing a  $\bar{D}^0 \rightarrow K^+\pi^-$  decay in events containing a tag anti-proton and where  $f_3$  is defined as the fraction of  $(\bar{D}|\bar{p})$  events not containing a  $\Lambda_c^+$ :

$$f_3 \equiv \frac{\mathcal{B}(c\bar{c} \rightarrow \bar{p} + \Theta'_c + X' + \bar{D})}{\mathcal{B}(c\bar{c} \rightarrow \bar{p} + X + \bar{D})} \quad (12)$$

in which  $\Theta'_c$  is a charm+baryon system other than a  $\Lambda_c^+$ . The main contributors to the numerator of this equation are events like  $e^+e^- \rightarrow \bar{D}DN\bar{p}X$  and, to a smaller, negligible extent, events in which a  $\Xi_c$  (Sect. IV A 3) is produced. Note that  $f_3$  is closely related to the previously defined  $f_1$  (Eqn. 5);  $f_1 \approx 1 + f_3$ .

It then follows that

$$\mathcal{B}(\Lambda_c^+ \rightarrow pK^-\pi^+) = \frac{\frac{\mathcal{Y}[\Lambda_c^+|\bar{p}] \cdot (1-f_2)}{\epsilon_{[\Lambda_c^+|\bar{p}]}}}{\frac{\mathcal{Y}(\bar{D}^0|\bar{p}) \cdot (1-f_3)}{\mathcal{B}(\bar{D}^0 \rightarrow K^+\pi^-) \cdot \epsilon_{(\bar{D}^0|\bar{p})}} + \frac{\mathcal{Y}(D^-\bar{p}) \cdot (1-f_3)}{\mathcal{B}(D^- \rightarrow K^+\pi^-\pi^-) \cdot \epsilon_{(D^-\bar{p})}} + \frac{\mathcal{Y}(D_s^-\bar{p}) \cdot (1-f_3)}{\mathcal{B}(D_s^- \rightarrow \phi\pi^-) \cdot \epsilon_{(D_s^-\bar{p})}}} \quad (13)$$

where, as before, particles contained in  $[\ ]$  are in the same hemisphere with respect to one another and particles contained in  $(\ )$  are in opposite hemispheres with respect to one another.

The major contributors to  $f_2$  are events containing  $\bar{\Lambda}_c\Lambda_c^+N\bar{p}$ . We measure the magnitude of this correction by measuring the yield of events containing a  $\bar{\Lambda}_c$  in the hemisphere opposite a tag anti-proton. Our equation for  $f_2$  is then

$$f_2 = \frac{\mathcal{Y}(\bar{\Lambda}_c|\bar{p})/\epsilon_{(\bar{\Lambda}_c|\bar{p})}}{\mathcal{Y}[\Lambda_c^+|\bar{p}]/\epsilon_{[\Lambda_c^+|\bar{p}]}} \quad (14)$$

The number of  $\bar{D}DN\bar{p}$  events are measured using  $S[D\bar{p}]$  same hemisphere correlations (Fig. 4; note that the  $DN$  combination here is the major component of what we previously referred to as “ $\Theta'_c$ ”); from these events, we compute  $f_3$ :

$$f_3 = \frac{\frac{\mathcal{Y}[D^0\bar{p}]}{\epsilon_{[D^0\bar{p}]} \cdot \mathcal{B}(D^0 \rightarrow K^-\pi^+)} + \frac{\mathcal{Y}[D^+\bar{p}]}{\epsilon_{[D^+\bar{p}]} \cdot \mathcal{B}(D^+ \rightarrow K^-\pi^+\pi^+)} + \frac{\mathcal{Y}[D_s^+\bar{p}]}{\epsilon_{[D_s^+\bar{p}]} \cdot \mathcal{B}(D_s^+ \rightarrow \phi\pi^+)}}{\frac{\mathcal{Y}(\bar{D}^0|\bar{p})}{\epsilon_{(\bar{D}^0|\bar{p})} \cdot \mathcal{B}(D^0 \rightarrow K^-\pi^+)} + \frac{\mathcal{Y}(D^-\bar{p})}{\epsilon_{(D^-\bar{p})} \cdot \mathcal{B}(D^+ \rightarrow K^-\pi^+\pi^+)} + \frac{\mathcal{Y}(D_s^-\bar{p})}{\epsilon_{(D_s^-\bar{p})} \cdot \mathcal{B}(D_s^+ \rightarrow \phi\pi^+)}} \quad (15)$$

In this equation, the full expression for  $\mathcal{Y}[D^0\bar{p}]$ , e.g., is

$$\mathcal{Y}[D^0\bar{p}] = \mathcal{L} \cdot \sigma(e^+e^- \rightarrow c\bar{c}) \cdot \mathcal{B}(c\bar{c} \rightarrow D^0 + \bar{p} + \Theta_c + X') \cdot \mathcal{B}(D^0 \rightarrow K^-\pi^+) \cdot \epsilon_{\bar{p}} \cdot \epsilon_{[D^0\bar{p}]} \quad (15a)$$

## B. Estimates of $f_2$ and $f_3$

### 1. $f_3$ and $D\bar{D}N\bar{p}$ backgrounds

There are two main contributors to  $f_3$ :  $D\bar{D}N\bar{p}$  events and fake tag antiprotons. They were previously discussed in the Tag Identification (Sect. III) and Triple Correlation Sections (Sect. IV), respectively. Both of these backgrounds inflate the calculated number of  $(\bar{D}|\bar{p})$  events (essentially the denominator of  $\mathcal{B}(\Lambda_c^+ \rightarrow pK^-\pi^+)$ , Eq.(13)) and thus will bias us towards a low final result if underestimated in the data. The  $D\bar{D}N\bar{p}$  background was found in both data and Monte Carlo using the plots shown in Figure 4 and a similar one for  $D_s^-$ . Monte Carlo simulations indicate that the  $\bar{p}$  in  $D\bar{D}N\bar{p}$  is equally likely to appear in the same hemisphere as the  $D$  as in the one opposite the  $D$ . Hence the number of events with  $D$  and  $\bar{p}$  in the same hemisphere were simply subtracted from the total number of events in the denominator of Eqn. (13) for  $\mathcal{B}(\Lambda_c^+ \rightarrow pK^-\pi^+)$ . Numerically, these backgrounds constitute  $(17 \pm 3)\%$  and  $(11 \pm 2)\%$  corrections to our initial  $(\bar{D}|\bar{p})$  sample in Monte Carlo and data, respectively, as indicated in Table I.

### 2. $f_3$ and $\Lambda_c^+\bar{\Lambda}_cN\bar{p}$ backgrounds

There is only one major contributor to  $f_2$ , namely  $\Lambda_c^+\bar{\Lambda}_cN\bar{p}$  events, as shown in Figure 13. These events are thought to be rare due to the energy needed to create the four baryons in such an event. However, it is possible that  $\bar{\Lambda}_c$  production is enhanced when a  $\Lambda_c^+$  is produced in an event. In order to estimate this effect we reconstruct events containing a  $\bar{p}$  opposite a  $\bar{\Lambda}_c$  and assume a charmed baryon opposite the  $\bar{\Lambda}_c$  (see Figure 14). The effect we see is approximately  $(7 \pm 3)\%$  in data. We therefore make an explicit correction of this magnitude ( $f_2$ ).

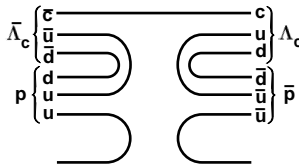


FIG. 13. Possible diagram for producing final states containing four baryons, including a  $\Lambda_c$  opposite a  $\bar{\Lambda}_c$ .

## C. Particle Reconstruction Efficiency and Tag Antiproton Fakes

In deriving  $\mathcal{B}(\Lambda_c^+ \rightarrow pK^-\pi^+)$ , we assume that the Monte Carlo simulation accurately reproduces the efficiency for reconstructing  $\Lambda_c^+$ 's, that is,  $\epsilon_{\Lambda_c^+}(\text{Data}) = \epsilon_{\Lambda_c^+}(\text{MC})$ .

Very approximately, the efficiency for reconstructing a tag antiproton in the  $O(\bar{p}|\bar{D})$ -tagged sample should equal the efficiency for reconstructing a tag antiproton in  $S[\bar{p}|\Lambda_c^+]$  events. However, the latter sample is obviously biased by the high momentum cut on the  $\Lambda_c^+$  ( $p_{\Lambda_c^+} > 2.5 \text{ GeV}/c$ ), which forces the same hemisphere antiproton tag into a low momentum regime (the kinematic upper limit on the momentum for a  $\bar{p}$  in a signal event to appear colinear with a  $\Lambda_c^+$  having  $p_{\Lambda_c^+} > 2.5 \text{ GeV}/c$  is

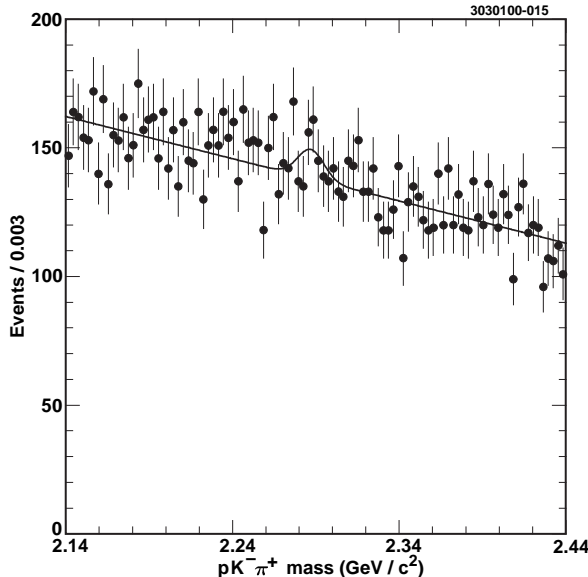


FIG. 14. Candidate  $\bar{\Lambda}_c$  mass (i.e.,  $pK^-\pi^+$  mass, in  $\text{GeV}/c^2$ ) for events containing a  $\bar{p}$  in the opposite hemisphere ( $\bar{p}\bar{\Lambda}_c$ ). The yield of this plot puts an upper limit on  $\Lambda_c^+\bar{\Lambda}_c N\bar{p}$  events.

1.65  $\text{GeV}/c$ ). In order to restrict the  $\Lambda_c^+$ 's to the same momentum interval in our  $O(\bar{p}|\bar{D})$  sample (denominator) as those in our  $S[\bar{p}\Lambda_c^+]$  sample (numerator), we restrict our calculation of final results to events in which tag antiprotons satisfy the requirement  $p_{\bar{p}} < 1.6 \text{ GeV}/c$ . This momentum cut therefore helps ensure that the  $\Lambda_c^+$  momentum spectrum in the denominator tag sample  $O(\bar{p}|\bar{D})$  is most similar to the  $\Lambda_c^+$  momentum spectrum in the  $S[\bar{p}\Lambda_c^+]$  sample, which constitutes the numerator in our double correlation ratio.

Below 1.6  $\text{GeV}/c$ , we must check that our tag antiprotons in the  $O(\bar{p}|\bar{D})$  sample have the same momentum spectrum as in our  $S[\bar{p}\Lambda_c^+]$  sample. If these subsamples are both drawn from the exact same parent ( $[\Lambda_c^+\bar{p}|\bar{D}]$ ) sample, then we certainly expect this to be the case. If the tag antiproton momentum spectrum for our  $O(\bar{p}|\bar{D})$  sample is the same as the tag antiproton momentum spectrum in our  $S[\bar{p}\Lambda_c^+]$  sample, then we are also insensitive to any possible variations in the antiproton-finding efficiency as a function of momentum.

Fake antiprotons can also contaminate our candidate antiproton tag sample, in a momentum-dependent manner. Figure 15 shows the likelihood of a kaon track to fake a proton track as a function of momentum, derived from  $\phi \rightarrow K^+K^-$  and  $D^0 \rightarrow K^-\pi^+$  events. Note that the rate at which pions fake protons is considerably smaller than the rate at which kaons fake protons (Figure 15) in the momentum interval of interest ( $p < 1.6 \text{ GeV}/c$ ), since kaons are closer in mass to protons than pions. Since pions tend to have random correlations with both  $D$ -mesons as well as  $\Lambda_c^+$ 's, pions faking protons largely cancel in both numerator and denominator of Eqn. 13. This is not necessarily the case for kaons faking protons.

In  $c\bar{c}$  events which do not contain charmed baryons, we expect a  $D$ -meson recoiling against the tag  $\bar{D}$ ; the  $D$ -meson will then decay into a negatively charged kaon ( $53 \pm 4\%$ ) of the time if the parent is a  $D^0$  and ( $24 \pm 3\%$ ) of the time if the parent is a  $D^+$  [7]. If the parent is a  $D_s$ ,  $K^-$  are produced ( $13 \pm 13\%$ ) of the time [7], hence the population of  $K^-$  potentially faking  $\bar{p}$  is enhanced in our  $\bar{D}$  tagged sample. Unfortunately, we have insufficient statistics to determine the level of

the fake tag background entirely from data, and we must rely on the Monte Carlo kaon and pion background fractions as a function of momentum to quantify antiproton fakes.

We thus use the following procedure to determine the contribution of fakes to our tag antiproton sample and then extract our final branching fraction:

1. We plot the tag anti-proton momentum spectrum, separately for our  $O(\bar{p}|\bar{D})$  and  $S[\bar{p}\Lambda_c^+]$  samples prior to any corrections (Figure 16). Since there is some background under the  $\Lambda_c^+$  and  $\bar{D}$  mass distributions, a sideband subtraction must be performed to remove background ( $pK^-\pi^+$ )- $\bar{p}$  correlations in the case of the  $S[\bar{p}\Lambda_c^+]$  sample, with a similar sideband subtraction for the  $O(\bar{p}|\bar{D})$  sample. The scaled antiproton momentum spectrum opposite  $K^+\pi^-$  invariant mass combinations in the  $\bar{D}^0$  sidebands ( $0.03 < |m_{K^+\pi^-} - m_{\bar{D}^0}| < 0.1$  GeV) is therefore subtracted from the antiproton momentum spectrum opposite  $K^+\pi^-$  invariant mass combinations in the  $\bar{D}^0$  signal region ( $|m_{K^+\pi^-} - m_{\bar{D}^0}| < 0.025$  GeV). We note in Figure 16 a large excess above the  $p < 1.6$  GeV/ $c$  kinematic limit, which we attribute, in part, to backgrounds from  $D\bar{D}N\bar{p}$  and kaons producing fake antiproton tags.
2. We now remove the contribution from non  $\bar{p}\bar{D}\Lambda_c^+$  events (in both data and Monte Carlo) to each of our  $O(\bar{p}|\bar{D})$  and  $S[\bar{p}\Lambda_c^+]$  samples (separately).
  - (a) We first subtract fake antiprotons using the measured kaon/pion fake rates as a function of momentum, multiplied by the kaon and pion production rates as a function of momentum. The per track fake rates are determined directly from data, as described previously. For the production momentum spectra, we rely on Monte Carlo simulations, which are based on the Particle Data Group  $D \rightarrow K^- X$  exclusive branching fractions and inclusive rates [7].
  - (b) We additionally subtract contributions due to  $D\bar{D}N\bar{p}$  and  $\Lambda_c^+\bar{p}N\bar{\Theta}_c$  from the fake-subtracted plot, using data for both of these estimates. These backgrounds are estimated from the yields in Figs. 4 and 14, respectively. The sideband-subtracted antiproton momentum spectra in our  $S[\bar{p}\bar{D}]$  and  $O(\bar{p}|\bar{\Lambda}_c^-)$  data samples are themselves directly subtracted from the signal  $O(\bar{p}|\bar{D})$  and  $S[\bar{p}\Lambda_c^+]$  antiproton momentum spectra. In doing so, we have removed backgrounds from  $D\bar{D}N\bar{p}$  and  $\Lambda_c^+\bar{p}N\bar{\Theta}_c$ .

After subtracting these backgrounds, we note improved agreement between the data tag antiproton spectrum for the  $O(\bar{p}|\bar{D})$  and  $S[\bar{p}\Lambda_c^+]$  samples. (Fig. 17).

3. After performing the above subtractions, we extract  $\mathcal{B}(\Lambda_c^+ \rightarrow pK^-\pi^+)$ , restricting ourselves to the interval where the Monte Carlo and data show good agreement for the  $\bar{p}$  momentum spectra (0.6–1.6 GeV/ $c$ ; as already mentioned, the upper momentum cut coincides with the kinematically allowed maximum momentum for our tag antiprotons given the minimum momentum requirement on the  $\Lambda_c^+$ ).

We take a combination of the magnitude of the fake subtraction and the spread in the derived values of  $\mathcal{B}(\Lambda_c^+ \rightarrow pK^-\pi^+)$  when we vary the limits of our tag antiproton momentum acceptance, as an estimate of the systematic error inherent in this procedure ( $\sim 15\%$ , Table II).

#### D. Checks of the $\bar{p}$ momentum spectrum

We have conducted a check of the double correlation analysis by using a sample of events which have the tag antiproton in the opposite (same) hemisphere of (as) the  $\Lambda_c^+$  ( $\bar{D}$ ), i.e., opposite to



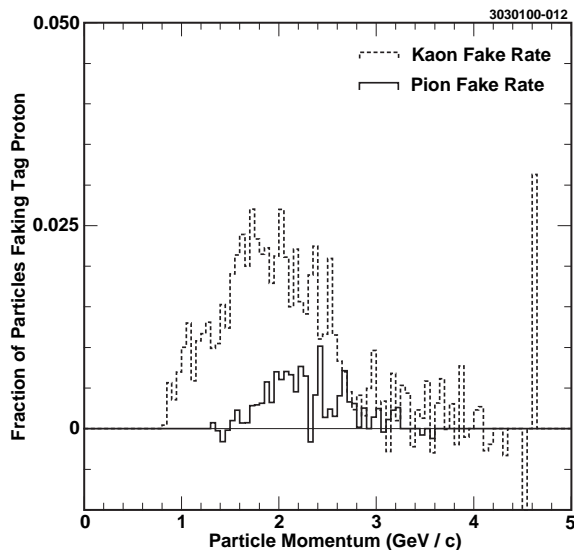


FIG. 15. The percentage of kaons and pions that pass all of our tag proton id requirements as a function of momentum. The data fake rate was found using kaons and pions from  $D^0 \rightarrow K^- \pi^+$  and  $\phi \rightarrow K^+ K^-$  decays as described in the text.

the correlation exploited in our standard analysis. Following the above notation, we denote these events as  $(\bar{p}\bar{D})|\Lambda_c^+$  events, and the subsample of those events which constitute the denominator and numerator in our double correlation sample as  $S[\bar{p}\bar{D}]$  and  $O(\bar{p}|\Lambda_c^+)$ , respectively. According to JETSET 7.3 simulations, approximately half of all  $\bar{p}\bar{D}\Lambda_c^+$  events will have the antiproton in the same hemisphere as the  $\Lambda_c^+$  (corresponding to our “standard” analysis), with the other half having the antiproton in the opposite hemisphere (see Fig. 8). We do not use these hemisphere/sign correlations in computing  $\mathcal{B}(\Lambda_c^+ \rightarrow pK^- \pi^+)$  for two main reasons - first, the level of  $D\bar{D}N\bar{p}$  is much more difficult to determine than for the standard  $O(\bar{p}\bar{D})$  sample, and second, the  $S[\bar{p}\Lambda_c^+]$  sample is very susceptible to  $\bar{\Lambda}_c\Lambda_c^+$  events in which there are no charmed mesons produced - in such a case, the tag antiproton can be a direct decay product of the  $\bar{\Lambda}_c$ . If we nevertheless trust the Monte Carlo to reproduce all backgrounds and efficiencies for this  $S[\bar{p}\bar{D}]$ -tagged data sample, and calibrate the observed yields in data to Monte Carlo simulations as above in the standard double correlation analysis, we obtain a central value for  $\mathcal{B}(\Lambda_c^+ \rightarrow pK^- \pi^+)$  which differs by  $\sim 12\%$  from the standard analysis (see Table II).

This  $(\bar{p}\bar{D})|\Lambda_c^+$  sample is much less susceptible to backgrounds from  $K^-$  which fake  $\bar{p}$  because the  $D$ , which would be the putative source of these fakes, is now fully reconstructed. The requirement that the tag antiproton now be found in the  $\bar{D}$  hemisphere rather than the  $\Lambda_c^+$  hemisphere biases the tag antiproton momentum spectrum in a different way than in the “standard” analysis. We can thus use these  $(\Lambda_c^+|\bar{p}\bar{D})$  events to qualitatively check our tag  $\bar{p}$  momentum spectra in the “standard”  $(\bar{p}\Lambda_c^+|\bar{D})$  analysis, after kaon fake subtraction in the standard analysis. The momentum spectrum for tag antiprotons in our cross-check  $(\Lambda_c^+|\bar{p}\bar{D})$  sample is shown in Figure 18. The antiproton momentum spectrum in the  $(\Lambda_c^+|\bar{p}\bar{D})$  sample is qualitatively similar to that in the standard  $(\Lambda_c^+|\bar{p}|\bar{D})$  analysis, after background corrections.

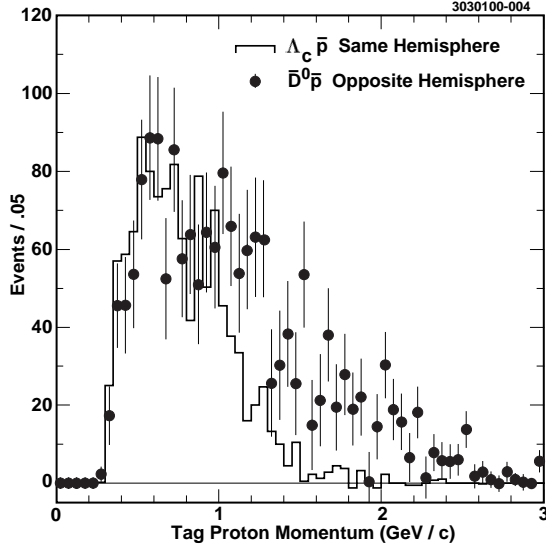


FIG. 16. Data tag antiproton momentum spectrum in  $[\Lambda_c^+ \bar{p}]$  same hemisphere events (solid histogram) and  $\bar{D}$  opposite  $\bar{p}$   $O(\bar{D}|\bar{p})$  events (points) in data, after a sideband subtraction on the  $\Lambda_c^+$  or  $\bar{D}$  mass, prior to subtracting tag anti-proton fakes. Notice the excess of high momentum tag antiprotons in the  $O(\bar{D}|\bar{p})$  sample.

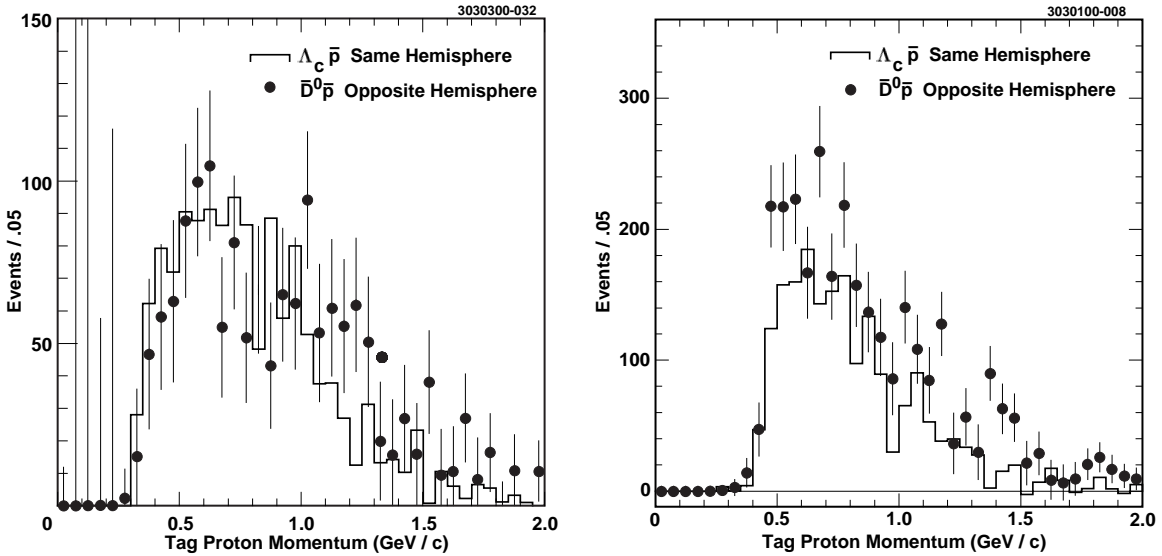


FIG. 17. Left: Previous plot after background subtractions. Tag anti-proton momentum in  $\Lambda_c^+ \bar{p}$  same hemisphere events ( $[\Lambda_c^+ \bar{p}]$ , solid histogram) and  $\bar{D}$  opposite  $\bar{p}$  events ( $O(\bar{D}|\bar{p})$ , points) in data after a sideband subtraction on the  $\Lambda_c^+$  or  $\bar{D}$  mass, and after subtracting tag antiproton fakes. Right: Corresponding Monte Carlo spectra, after similar subtractions, for comparison.

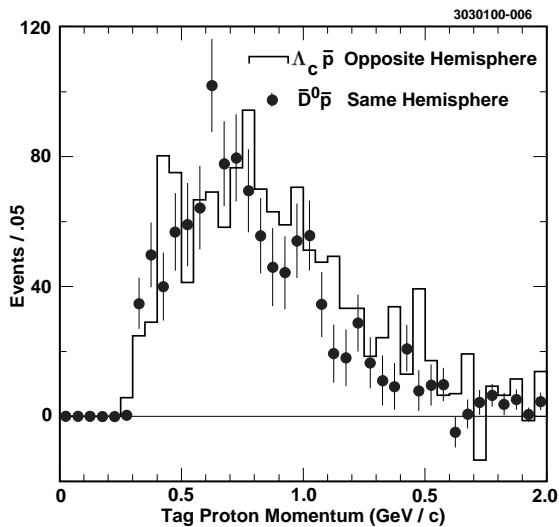


FIG. 18. Cross-check results. Tag antiproton momentum in  $O(\Lambda_c^+ \bar{p})$  opposite hemisphere events (solid histogram) and  $S[\bar{D} \bar{p}]$  same hemisphere events (points) in data, after a sideband subtraction on the  $\Lambda_c^+$  or  $\bar{D}^0$  mass. This sample should be less susceptible to tag proton fakes, since the sign correlation is not correct for kaons coming from semileptonic charm decay to fake antiprotons, as was the case for our  $\bar{D}$  opposite  $\bar{p}$  event sample. However, we do not use these hemisphere/sign correlations in computing  $\mathcal{B}(\Lambda_c^+ \rightarrow p K^- \pi^+)$  due to the difficulty in estimating the  $D \bar{D} N \bar{p}$  and  $\Lambda_c^+ \bar{\Lambda}_c$  backgrounds in this event sample.

## VI. RESULTS

Our results, showing the yields  $\mathcal{Y}$ , efficiencies  $\epsilon$ , and backgrounds, in both data and Monte Carlo, are tabulated in Table I. The weighted average of the three techniques corresponds to  $\mathcal{B}(\Lambda_c^+ \rightarrow pK^-\pi^+) = (5.0 \pm 0.5)\%$  (statistical error only).

TABLE I. Event yields for signal and backgrounds, in data and Monte Carlo. As before, same hemisphere correlations are designated with brackets [ ], and opposite hemisphere correlations are designated with parenthesis ( ). Background yields which are subtracted from the numerator or denominator are indicated with a minus sign.

Double Correlations	MC	Data
$\mathcal{Y}[\Lambda_c^+ \bar{p}]$ (Numerator)	1656±65	1093±47
$\mathcal{Y}(\bar{D}^0   \bar{p})$ (Denominator)	2725±84	1369±55
$\mathcal{Y}(D^-   \bar{p})$ (Denominator)	1501±113	963±71
$\mathcal{Y}(D_s^-   \bar{p})$ (Denominator)	111±19	51±11
$\epsilon_{\Lambda_c^+} / \epsilon_{D^0} / \epsilon_{D^-} / \epsilon_{D_s^-}$	26.5%/43.7%/32.2%/14.5%	
$\mathcal{Y}(\bar{\Lambda}_c   \bar{p})$ (Bkgnd to Num.)	-84±49	-75±39
$\mathcal{Y}[D^0 \bar{p}]$ (Bkgnd to Den.)	-268±40	-68±23
$\mathcal{Y}[D^+ \bar{p}]$ (Bkgnd to Den.)	-417±67	-152±39
$\mathcal{Y}[D_s^+ \bar{p}]$ (Bkgnd to Den.)	-26±11	-1±6
fake $\bar{p}$ in $[D\bar{p}]$ evts. (Bkgnd. to Den.)	-272±31	-298±36
$f_2$	(5.1 ± 2.9)%	(6.9 ± 2.2)%
$f_3 (\approx f_1 - 1)$	(17.5 ± 3.4)%	(10.6±2.4)%
$\mathcal{B}(\Lambda_c^+ \rightarrow pK^-\pi^+)$	4.3% (input)	(4.9±0.5)%
$(\pi_{\text{soft}}^-   \bar{p})$ Triple Correlation		
$\mathcal{Y}(\pi_{\text{soft}}^-   \bar{p})$ (Denominator)	34222±1092	14553±485
fake $\bar{p}$ in $(\pi_{\text{soft}}^-   \bar{p})$	-3318±310	-1867 ± 261
$\mathcal{Y}([\Lambda_c^+ \bar{p}]   \pi_{\text{soft}}^-)$ (Numerator)	202.8±27.8	101.6±20.6
$\mathcal{B}(\Lambda_c^+ \rightarrow pK^-\pi^+)$	4.3% (input)	(5.2±1.3)%
$(e^-   \bar{p})$ Triple Correlation		
$\mathcal{Y}(e^-   \bar{p})$ (Denominator)	4178±65	1739±47
fake $\bar{p}$ + fake $e^-$	-382±39	-272 ± 41
$\mathcal{Y}([\Lambda_c^+ \bar{p}]   e^-)$ (Numerator)	20.1±5.2	10.3±3.8
$\mathcal{B}(\Lambda_c^+ \rightarrow pK^-\pi^+)$	4.3% (input)	(5.6±2.5)%

## VII. SUMMARY OF SYSTEMATIC UNCERTAINTIES

We have already discussed many of the systematic errors and their assessment in previous sections. Table II lists the systematic errors evaluated for the three methods of extracting  $\mathcal{B}(\Lambda_c^+ \rightarrow pK^-\pi^+)$ . As discussed previously, the largest systematic error is due to uncertainties in the tagging efficiency and spectrum. This includes possible backgrounds to the antiproton tags, and the difference between the  $\bar{p}$  momentum spectra in  $S[\Lambda_c\bar{p}]$  and  $O(\bar{D}|\bar{p})$  events. Uncertainties in backgrounds and tagging efficiencies are assessed, in part, by varying the tag antiproton momentum interval over which our final result is extracted by  $\pm 300$  MeV/c in either direction from the default value. The error (“Event Selection/MC Mismodeling”) is evaluated by varying the event selection criteria for both data and Monte Carlo and determining the variation in the calculated final result. This error also includes the discrepancy between the central value we quote and the result obtained from the cross-check in which the antiproton is identified in the same hemisphere as the charm tag. It also includes the variation in the final result obtained using different versions of charged track reconstruction software, comparing the internal consistency of different data subsamples, and different versions of the Monte Carlo event generator and detector simulation.

TABLE II. Summary of systematic errors assessed in measurement of  $\mathcal{B}(\Lambda_c^+ \rightarrow pK^-\pi^+)$ .

	$\pi_{\text{soft}}$ tag	Electron tag	Double Corr.
Tag proton id/spectrum	15%	15%	15%
Event Selection/MC Mismodeling	15%	14%	12%
$D\bar{D}N\bar{p}$ background events	8%	8%	8%
$\Lambda_c^+/D$ momentum spectra	8%	8%	8%
$\Lambda_c^+/D$ id cuts	5%	5%	5%
$\Lambda_c^+$ mass fit/sideband subtraction	6%	10%	1%
Contamination from $\Sigma_c^0, \Lambda_{cJ}$	6%	-	-
tag electron fakes	-	5%	-
$\Lambda_c^+\bar{\Lambda}_cN\bar{p}$ events	-	-	4%
$\mathcal{B}(D^0 \rightarrow K^-\pi^+)$	-	-	2%
$\mathcal{B}(D^+ \rightarrow K^-\pi^+\pi^+)$	-	-	3%
Beam-wall/Beam-gas contamination	3.5%	3.5%	3.5%
Contamination of $\Xi_c, \Omega_c$ events	3%	3%	3%
Hemisphere Correlation	2%	2%	2%
Total	28%	25%	24%

## VIII. DISCUSSION AND CONCLUSIONS

Employing new techniques of baryon-charmed particle correlations in  $e^+e^- \rightarrow c\bar{c}$  annihilations at a center of mass energy  $\sqrt{s} \sim 10.55$  GeV, we measure  $\mathcal{B}(\Lambda_c^+ \rightarrow pK^-\pi^+) = (5.0 \pm 0.5 \pm 1.2)\%$ . At present, this technique is limited by our understanding of the non-signal backgrounds (most notably,  $D\bar{D}N\bar{p}$  backgrounds); presumably, more data would allow a greater understanding of those backgrounds. Our result is consistent with the determination of  $\mathcal{B}(\Lambda_c^+ \rightarrow pK^-\pi^+) = 7 \pm 2\%$

suggested by Dunietz [6], based on the measured ratio for  $\mathcal{B}(\Lambda_c^+ \rightarrow \Lambda X l \nu)/\mathcal{B}(\Lambda_c^+ \rightarrow p K^- \pi^+)$  and assuming that the semileptonic charmed baryon width is the same as the semileptonic charmed meson width. It is also consistent with the value of  $(5.0 \pm 1.3)\%$  derived by the Particle Data Group [7]. We now discuss the implications of this result and its consistency with related measurements.

The product branching fraction:  $\mathcal{B}(B \rightarrow (\Lambda_c^+ X \text{ or } \bar{\Lambda}_c X)) \cdot \mathcal{B}(\Lambda_c^+ \rightarrow p K^- \pi^+)$  can be directly determined by simply measuring the efficiency-corrected  $\Lambda_c^+ \rightarrow p K^- \pi^+$  yield in  $B\bar{B}$  events. An unpublished CLEO result finds a value of  $\mathcal{B}((B + \bar{B}) \rightarrow \Lambda_c^+) \cdot \mathcal{B}(\Lambda_c^+ \rightarrow p K^- \pi^+) = (1.81 \pm 0.22 \pm 0.24) \times 10^{-3}$  [16] for this product branching fraction. Given that,  $\mathcal{B}(\Lambda_c^+ \rightarrow p K^- \pi^+) = 0.05$  implies that  $\mathcal{B}(B \rightarrow (\Lambda_c^+ \text{ or } \bar{\Lambda}_c)) \sim 3.6\%$ . This can be compared to the Particle Data Group value of  $\mathcal{B}(B \rightarrow p \text{ or } \bar{p}) \sim 8.0\%$  [7]. Our result therefore implies that  $B \rightarrow \text{baryons}$  may be occurring at a substantial rate through modes such as  $\bar{B} \rightarrow D N \bar{N} X$  [17],  $\bar{B} \rightarrow \Xi_c \bar{Y} X$ , or  $\bar{B} \rightarrow \Xi_c \bar{\Lambda}_c$ . CLEO has recently published evidence for the latter modes [18].

We can also place bounds on the  $\Lambda_c^+ \rightarrow p K^- \pi^+$  branching fraction by using the measured CLEO  $e^+e^- \rightarrow \text{hadrons}$  cross-section, assuming that the  $c\bar{c}$  fraction is 40% of the total hadronic cross-section. CLEO has measured  $\mathcal{B}(\Lambda_c^+ \rightarrow p K^- \pi^+) \cdot \sigma(e^+e^- \rightarrow (\Lambda_c^+ + \bar{\Lambda}_c)) = 10 \pm 1$  pb. That measurement simply determines the total yield of either  $\Lambda_c^+$  or  $\bar{\Lambda}_c$  in  $e^+e^-$  annihilations; i.e., it determines the sum of  $c \rightarrow \Lambda_c^+$  plus  $\bar{c} \rightarrow \bar{\Lambda}_c$ . Our value of  $\mathcal{B}(\Lambda_c^+ \rightarrow p K^- \pi^+) = 0.05$  implies that  $\sigma(e^+e^- \rightarrow (\Lambda_c^+ + \bar{\Lambda}_c)) = 200$  pb. Using the recent CLEO measurement of  $R \equiv \frac{\sigma(e^+e^- \rightarrow q\bar{q})}{\sigma(e^+e^- \rightarrow \mu^+\mu^-)}$  [19], which corresponds to a value of  $\sigma(e^+e^- \rightarrow q\bar{q}) \sim 3.3$  nb, and using the JETSET value of  $c \rightarrow \Lambda_c^+ \sim 0.07$ , we have:  $\sigma(e^+e^- \rightarrow q\bar{q}) \times \frac{c\bar{c}}{q\bar{q}} \times (c \rightarrow \Lambda_c^+ + \bar{c} \rightarrow \bar{\Lambda}_c) = 3300 \text{ pb} \times 0.4 \times 0.07 \times 2 = 185$  pb, in good agreement with our measurement above.

Finally, since the presently tabulated exclusive  $\Lambda_c^+$  decays are all normalized to  $\mathcal{B}(\Lambda_c^+ \rightarrow p K^- \pi^+)$ , we conclude that  $\sim 50\%$  of the  $\Lambda_c^+$  width is unaccounted for. Since the  $\Lambda_c^+$  lifetime is only  $\sim 40\%$  of the  $D^0/D_s$  lifetime, it has long been realized that diagrams such as exchange diagrams, and/or final states including neutrons, are likely to be large contributors to  $\Lambda_c^+$  decay and may produce final states different than the ‘usual’ states expected from simple  $\Lambda_c^+ \rightarrow \Lambda W_{\text{external}}$  diagrams. Measurement of such decays await additional data and analysis.

## ACKNOWLEDGMENTS

We gratefully acknowledge the effort of the CESR staff in providing us with excellent luminosity and running conditions. J.R. Patterson and I.P.J. Shipsey thank the NYI program of the NSF, M. Selen thanks the PFF program of the NSF, M. Selen and H. Yamamoto thank the OJI program of DOE, J.R. Patterson, K. Honscheid, M. Selen and V. Sharma thank the A.P. Sloan Foundation, M. Selen and V. Sharma thank the Research Corporation, F. Blanc thanks the Swiss National Science Foundation, and H. Schwarthoff and E. von Toerne thank the Alexander von Humboldt Stiftung for support. This work was supported by the National Science Foundation, the U.S. Department of Energy, and the Natural Sciences and Engineering Research Council of Canada.

## REFERENCES

- [1] H. Albrecht *et al.* (The ARGUS Collaboration), Phys. Lett. **B269**, 234 (1991).
- [2] T. Bergfeld *et al.* (The CLEO Collaboration), Phys. Lett. **B323**, 219 (1994).
- [3] M. A. Ivanov *et al.*, hep-ph/9910342, and references cited therein.
- [4] G. Crawford *et al.*, (The CLEO Collaboration), Phys. Rev. **D45**, 752 (1992), and M. Procario *et al.*, Phys. Rev. Lett. **73**, 1472 (1994).
- [5] H. Albrecht *et al.* (The ARGUS Collaboration), Z. Phys. **C58**, 191 (1993), and H. Albrecht *et al.* (The ARGUS Collaboration), Z. Phys. **C42**, 191 (1989).
- [6] I. Dunietz, hep-ph/9805287, and Phys. Rev. **D58** 094010 (1998).
- [7] The Particle Data Group, Eur. Phys. J. **C3**, 1 (1998).
- [8] R. Ammar *et al.* (The CLEO Collaboration), Phys. Rev. **D55**, 13 (1997).
- [9] Y. Kubota *et al.*, (The CLEO Collaboration), Nucl. Instrum. Methods Phys. Res. **A320**, 66 (1992).
- [10] G. Fox and S. Wolfram, Phys. Rev. Lett. **41**, 1581 (1978).
- [11] G. Crawford *et al.*, Nucl. Instrum. Meth. **A345**, 429, (1994).
- [12] S. Brandt and H.D. Dahmen, Z. Phys. **C1**, 61 (1979).
- [13] D. Akerib *et al.* (The CLEO Collaboration), Phys. Rev. Lett. **71**, 3070 (1993).
- [14] JETSET 7.3: T. Sjöstrand and M. Bengtsson, Comput. Phys. Commun. **43**, 367 (1987).
- [15] R. Brun *et al.*, “GEANT3 Users Guide,” CERN DD/EE/84-1 (1987).
- [16] M. Zoeller, Ph. D. Thesis, State University of New York, Albany, 1994 (unpublished).
- [17] I. Dunietz, FERMILAB -CONF-97-230-T, hep-ph/9708252, Mar. 1997, and Proceedings of the 2nd International Conference on B physics and CP violation, Honolulu, Hawaii, 24-27 March 1997.
- [18] B. Barish *et al.* (The CLEO Collaboration), Phys. Rev. Lett. **79**, 3599 (1997).
- [19] R. Ammar *et al.* (The CLEO Collaboration), Phys. Rev. **D57**, 1350 (1998). The cross-section quoted here is, of course, approximate since we do not specify the infrared cutoff for initial state radiation.